Engineering of Transition Metal Catalysts Confined in Zeolites

Kosinov, Nikolay; Liu, Chong; Hensen, Emiel J.M.; Pidko, Evgeny A.

DOI
10.1021/acs.chemmater.8b01311

Publication date
2018

Document Version
Final published version

Published in
Chemistry of Materials

CHEMISTRY OF MATERIALS
Cite This: Chem. Mater. 2018, 30, 3177−3198
Review
pubs.acs.org/cm

Engineering of Transition Metal Catalysts Confined in Zeolites

Nikolay Kosinov,*[,†,∥] Chong Liu,[†] Emiel J. M. Hensen,*[,‡] and Evgeny A. Pidko*[,†,§]

[†]Inorganic Systems Engineering Group, Department of Chemical Engineering, Faculty of Applied Sciences, Delft University of Technology, Van der Maasweg 9, 2629 HZ Delft, The Netherlands

[‡]Schuit Institute of Catalysis, Laboratory of Inorganic Materials Chemistry, Eindhoven University of Technology, P.O. Box 513, 5600 MB Eindhoven, The Netherlands

[§]TheoMAT group, ITMO University, Lomonosova str. 9, St. Petersburg 191002, Russia

ABSTRACT: Transition metal−zeolite composites are versatile catalytic materials for a wide range of industrial and lab-scale processes. Significant advances in fabrication and characterization of well-defined metal centers confined in zeolite matrixes have greatly expanded the library of available materials and, accordingly, their catalytic utility. In this review, we summarize recent developments in the field from the perspective of materials chemistry, focusing on synthesis, postsynthesis modification, (operando) spectroscopy characterization, and computational modeling of transition metal−zeolite catalysts.

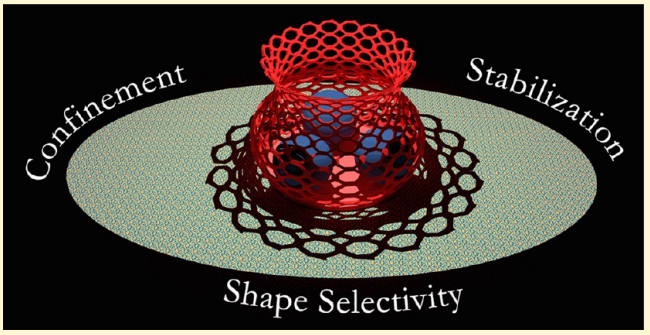

INTRODUCTION

Why Zeolites? Single-site catalysts are the materials to bridge the gap between homogeneous (highest activity per active site, well-defined active sites, proper reaction mechanistic understanding) and heterogeneous (cheap, recyclable, and stable catalysts) branches of the catalysis science.[1−3] Zeolite-based catalysts are important members of the single-site heterogeneous catalysts' family.[4] First of all, the pores and channels of molecular dimensions bring about the shape selectivity; that is, the reactions inside zeolites depend on how well the products/intermediates/reactants fit within the pores.[5,6] Second, small pores of zeolites allow preparation of well-defined nanoparticles and sub-nanoparticles of catalytically active transition metals. Further, isomorphously substituted zeolites contain catalytically active Brønsted and/or Lewis acid sites that are also suitable for the coordination of highly dispersed transition metal centers. Finally, the relatively high (hydro-)thermal stability of zeolites allows for performing reactions under harsh conditions in both gas and liquid phases.[7−10] All of these properties make zeolites preferable catalytic materials for many industrially and environmentally important reactions. The catalytic applications of zeolites have been extensively discussed in a number of excellent reviews devoted to such processes as oil refinery,[11,12] biomass conversion,[13,14] direct valorization of natural gas,[15,16] methanol-to-hydrocarbons process,[17−19] and selective catalytic reduction of nitrogen oxides.[20−22]

Synthesis of transition metal moieties inside the zeolite pores is challenging since typical organometallic purification approaches of recrystallization, extraction, or distillation are not applicable. The preparation of such moieties must be therefore intrinsically selective. To achieve this, the molecular factors that govern the formation and stability of particular inorganic species inside the zeolite pores need to be understood. This review focuses on the material science aspects of the synthesis and understanding of well-defined transition metal catalysts confined in zeolites. The review is organized as follows. We first introduce the general aspects of metal encapsulation inside the zeolite pores and discuss the main advantages of zeolites compared to nonmicroporous carriers. Then key synthesis techniques together with various chemical and structural modification approaches used in zeolite chemistry will be reviewed. This will be followed by the discussion of the recent advances in physical-chemical characterization and computational modeling of metal−zeolite composites. The final section of this review will present a general summary and provide an outlook on the future of the multiscale engineering of zeolite-based catalysts.

Zeolite-Based Well-Defined Transition Metal Catalysts. Zeolites are crystalline microporous silicate materials. There are currently over 230 zeolite topologies listed in the Database of Zeolite Structures.[23] The variety of pore architectures results in different pore sizes, dimensionality of the channel system (from 0D to 3D), cages, pockets, and other structural features (Figure 1). From the catalytic perspective, these features greatly influence the chemical reactions, occurring within the microporous space, mainly because of shape-selectivity effects and coordination of active metal sites. It is possible to exploit the shape selectivity and specific metal−

Received: March 29, 2018
Revised: April 26, 2018
Published: May 7, 2018

DOI: 10.1021/acs.chemmater.8b01311
Chem. Mater. 2018, 30, 3177−3198

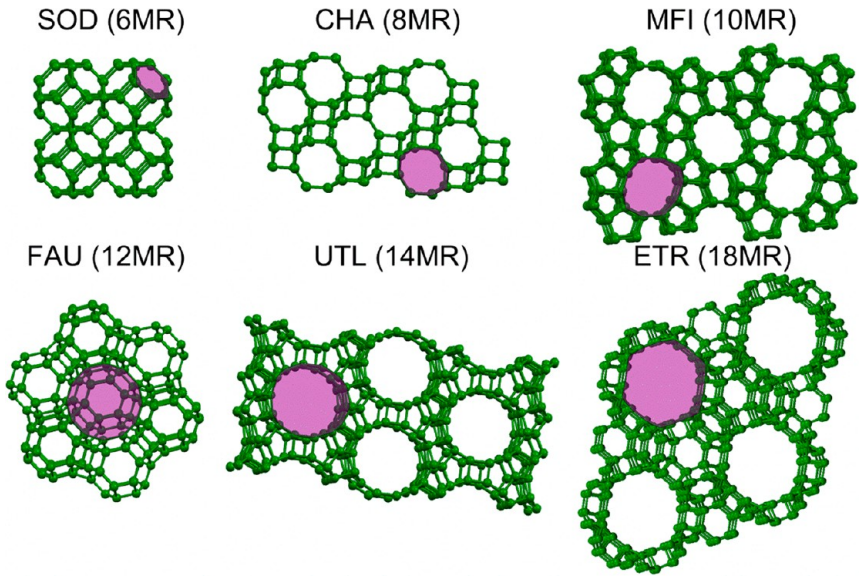

Figure 1. Zeolite topologies with different pore architectures: SOD with 6-membered ring (6MR) pores of 2.8 Å; CHA (3.8 Å); MFI (~5.5 Å); FAU (7.4 Å); UTL (~9.5 Å); and ETR (10.1 Å).

zeolite interaction to prepare well-defined and highly effective catalysts.

Shape Selectivity. Shape selectivity is a unique feature of crystalline microporous materials that frequently has a great impact on their catalytic performance, even allowing for certain reactions to be performed that would otherwise have been impossible. A relevant example is methane dehydroaromatization (MDA) which represents an attractive technology for the direct valorization of natural gas. This reaction is catalyzed by highly dispersed semireduced Mo sites stabilized within the zeolites micropores. Non-zeolitic materials are not efficient for the MDA reaction and only lead to the formation of graphitic compounds (coke). The superior performance of the zeolite catalysts is associated with three main factors: (i) high thermal stability of the zeolite carrier, (ii) strong metal−support interactions, and (iii) suitable shape-selectivity properties. Thermodynamics dictates that non-oxidative conversion of methane to benzene can only be achieved at very high temperature (>700 °C). This makes the thermally stable zeolites suitable supports for the active Mo phase. Further, since the reduced Mo centers tend to agglomerate and form large and inactive particles at elevated temperatures, the strong interaction between the metal and the $[AlO_4]^-$ tetrahedra are crucial for the efficacy of Mo/zeolite composites.[24] Last and most important, the confinement of the Mo sites inside the pores of the appropriate size is imperative for the selective formation of benzene and not the thermodynamically favored coke.[25] Figure 2 demonstrates the catalytic performance of 5% Mo/zeolite catalysts of the same chemical composition, but varying pore dimensions.[26] Only when Mo centers were dispersed in the channels of MFI zeolite (pore diameter ca. 5.5 Å, size of benzene molecule ca. 5.5 Å) was a significant production of benzene observed. Clearly, MFI pores are large enough for benzene to diffuse out, while being small enough to hinder the extensive formation of polyaromatic species eventually blocking the pores. Mo/MOR with pores of about 7 Å displays low benzene selectivity because they cannot restrict the growth of two-dimensional polyaromatics. In turn, the low efficiency of Mo/CHA is related to the inability of benzene to leave the small (3.8 Å) pore openings.

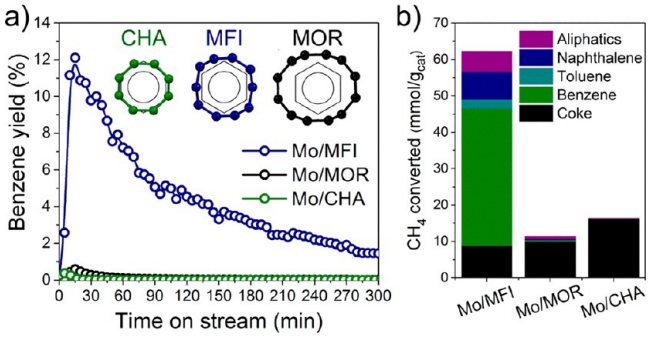

Figure 2. Results of methane dehydroaromatization (MDA) tests over 5%Mo/zeolite catalysts with the same chemical composition. Benzene yields with the inset demonstrating pore openings of corresponding zeolites (a) and overall product distributions obtained during 16 h tests (b). Conditions: 700 °C, atmospheric pressure, 0.3 g of catalyst, CH_4 WHSV 2.0 h^{-1}. Adapted with permission from ref 26. Copyright 2016 American Chemical Society.

Another representative example of the shape-selectivity effects is provided by a recent work of Zhang et al., who encapsulated Pd nanoparticles inside the 12MR pores of zeolite Beta (BEA) to obtain an efficient catalyst for the selective hydrogenation of functionalized nitroarenes.[27] Pd@Beta catalyst displayed a remarkable selectivity to functionalized aminoarenes (Figure 3). Importantly, Pd@Beta significantly outperformed the benchmark Pd/C catalyst in terms of catalytic stability. The authors attributed the observed drastic activity enhancement for Pd@Beta to the sterically selective substrate adsorption inside the zeolite channels, which favors the interaction between the nitro group and the active Pd species.

The shape-selectivity effects are very common in the field of zeolite catalysis. Besides the product selectivity discussed above, shape selectivity toward reagents, intermediates, and even poisons in zeolite catalysts have been reported.[28,29] The ability of zeolite architectures to stabilize/confine organocatalytic molecules enables the fascinating chemistry of a hydrocarbon pool mechanism.[30,31] This reaction pathway is at the basis of

DOI: 10.1021/acs.chemmater.8b01311
Chem. Mater. 2018, 30, 3177−3198

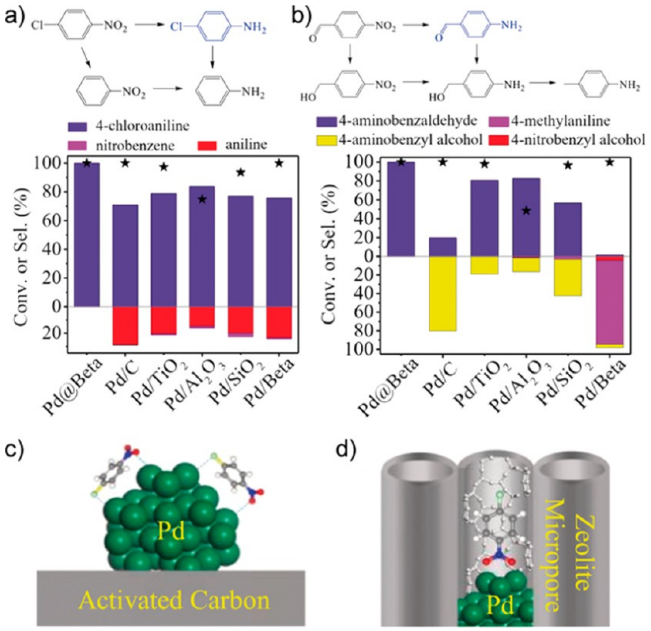

Figure 3. Substrate conversions (★) and product selectivities (colored columns and numerical values) for the hydrogenation of variously substituted nitroarenes and chlorobenzaldehyde on various catalysts. Adapted with permission from ref 27. Copyright 2017 Wiley.

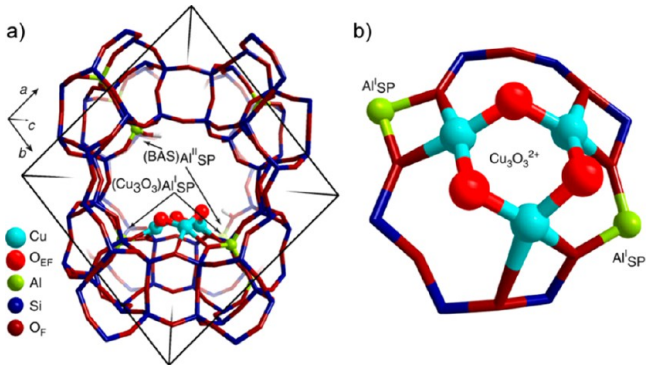

Figure 4. Structure and location of $[Cu_3(\mu\text{-}O)_3]^{2+}$ cluster in mordenite predicted by density functional theory (DFT) modeling. The zeolite model contained paired (type I) and isolated (type II) Al atoms located at the pore mouth of the side pocket. The cluster is stabilized by two anionic centers due to Al^{I}_{SP} lattice sites at the entrance of the MOR side pocket (b) so that the extraframework oxygens responsible for the initial C−H activation are pointing toward the main channel of MOR (a). The charge due to the remaining Al^{II}_{SP} is compensated by acidic protons resulting in BAS formation. Adapted with permission from ref 36. Copyright 2015 Macmillan Publishers Limited.

the methanol-to-hydrocarbon conversion processes, and it has recently been found to play a role in the MDA reaction as well.[32] To enable the advantageous shape-selectivity effects during catalytic reaction over transition metal sites, the latter should remain inside the pores. This can be complicated because initially dispersed metal atoms/clusters tend to diffuse out of the pores and agglomerate on the zeolite external surface. In the next sections, we will discuss how the intrinsic chemical and physical properties of the zeolite frameworks can be exploited to stabilize the well-defined metal centers.

Coordination and Encapsulation of Active Sites. Isomorphous substitution of Si atoms in the zeolite framework by trivalent elements (typically Al, although B, Fe, and Ga can also be applied) introduces a negative charge on the lattice that needs to be balanced by a positively charged counterion. When the charge-balancing is provided by a proton, a Brønsted acid site is formed.[33] Alternatively, the negative lattice charge can be balanced by any other cationic species including a metal cation or a cationic metal complex giving rise to isolated and often catalytically active transition metal centers, i.e., single-site catalysts. Polynuclear copper-oxo clusters stabilized by the zeolite $[AlO_4]^-$ tetrahedra exemplify this concept.

These clusters mimic copper-oxo complexes that are present in methane monooxygenase and are very efficient catalysts for the selective oxidation of methane to methanol,[34] among other applications.[35] Figure 4 shows a $[Cu_3(\mu\text{-}O)_3]^{2+}$ complex stabilized by two $[AlO_4]^-$ tetrahedra at the pore mouth of an 8MR side pocket of zeolite MOR. Grundner et al. prepared these well-defined complexes by ion-exchange of an H-form MOR zeolite with an aqueous solution of copper(II) acetate, followed by a thermal activation in oxygen flow. Due to a high concentration of uniform Cu-oxo clusters stabilized in a relatively low-silica MOR zeolite matrix (Si/Al = 11), the obtained Cu-MOR catalyst demonstrated a remarkable activity, selectivity, and recyclability in a two-step oxidation of methane to methanol.[36] The authors hypothesized that the proper confinement of the Cu-oxo clusters at the side pockets of MOR contributed to the enhanced activity as well.

In addition to chemical stabilization via strong basic lattice sites ligation,[37,38] zeolites can stabilize the metal centers mechanically, that is by encapsulating them. Diffusion of metal atoms/clusters through small zeolite pores is significantly restricted as compared to open surfaces of typical supports. Once the active phase is dispersed inside the zeolite, whether *in situ* or during a postsynthesis modification, the zeolite framework will protect it from sintering even at elevated temperatures. Li et al.[39] employed such an approach to prepare Pt nanoparticulate catalysts with an exceptional thermal stability. Figure 5 shows electron microscopy images and corresponding size distributions of Pt nanoparticles dispersed inside nanoshells formed by the MFI zeolite and on a conventional silica support activated at different temperatures. Encapsulation inside the zeolite pores makes Pt@nanoshell material completely stable against the metal phase sintering even under reductive conditions at a temperature as high as 750 °C. This finding highlights one of the key advantages of metal−zeolite hybrids: strong stabilization of the active transition metal phase by the crystalline zeolite framework.

■ ENGINEERING WELL-DEFINED ZEOLITE CATALYSTS

Given the extreme breadth of the field of zeolite catalysis, a thorough and complete discussion of all the relevant reactions that can be catalyzed by transition metal−zeolite composites is neither practical nor realistic within this review. Table 1 shows some selected applications, interesting from industrial, fundamental, or environmental perspectives. We encourage an interested reader to refer to the review papers and book chapters we refer to in Table 1 for a detailed discussion and extensive literature overview.

Metals from across the periodic table have been confined inside the zeolite pores. Figure 6 shows distribution of indexed publications, related to specific elements, applied as catalysts in combination with zeolites. The largest number of articles expectedly belong to the proton forms of Al-containing

DOI: 10.1021/acs.chemmater.8b01311
Chem. Mater. 2018, 30, 3177−3198

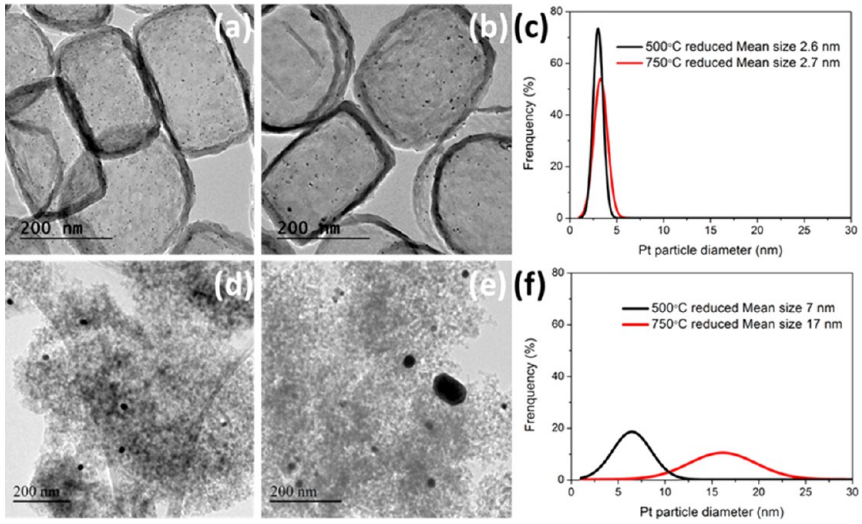

Figure 5. Transmission electron microscopy (TEM) images of Pt@nanoshell reduced at 500 °C for 2 h (a) and 750 °C for 10 h (b) under H_2 and Pt particle size distributions of the two materials (c). TEM images of a commercial Pt/SiO_2 catalyst reduced at 500 °C (d) and 750 °C (e) under the same conditions as those for Pt@hollow and Pt particle size distributions (f) of the two materials in (d) and (e). The particle size distributions have been modeled using a Normal law from the measurements on 400 particles. Adapted with permission from ref 39. Copyright 2015 Elsevier.

Table 1. Selected Catalytic Applications of Transition Metal–Zeolite Composites, with Active Metals Listed Separately

selected applications	metals	ref
oil processing		
hydrocracking	Ni/Mo, Ni/W, Pt, Pd	40
naphtha reforming	Pt (promoted with Re, Sn, Ir, Ge, etc.)	41
paraffin aromatization	Ga, Zn, Ag	42
natural gas processing		
methane dehydroaromatization	Mo, Re, Fe	43
selective oxidation of methane to methanol	Cu, Fe	44
biomass conversion		
conversion of carbohydrates to 5-hydroxymethylfurfural, γ-valerolactone, and lactic acid	Sn, Ti, Zr	45
environmental applications		
selective catalytic reduction (SCR) of nitrogen oxides ($deNO_x$)	Cu, Fe, Ag, Co	46
(photo-)catalytic removal of volatile organic compounds (VOC)	Ti, Cu, Pt, Pd	47
deep catalytic oxidation of water pollutants	Cu, Fe	48
catalytic combustion of CO and hydrocarbons	Pd, Ni	49
synthesis of chemicals and chemical building blocks		
shape-selective/bifunctional Fischer–Tropsch synthesis	Co, Fe, Ru	50
olefin epoxidation	Ti,	51
benzene to phenol oxidation with N_2O	Fe, Ti	52
selective hydrogenation of nitroarenes	Pd, Pt	53
Diels–Alder reactions	Zn, Cr, Ga, Cu, Zr	54
Baeyer–Villiger oxidation of ketones, Meerwein–Ponndorf–Verley–Oppenauer reactions	Sn, Ti, Zr	55

zeolites—typical Brønsted acid catalysts that reside outside of the scope of this review. Among transition metals, such catalytically prominent elements as Cu, Pt, Fe, Ni, Ti, Pd, Co, and Mo are expectedly on top of the list.

Figure 7 schematically illustrates three conceptually different transition metal–zeolite composites:

(i) Isolated metal (oxide, carbide, nitride) (sub-)-nanoparticles.
(ii) Ion-exchanged cations, mono- or oligonuclear (oxo) complexes, stabilized on the $[AlO_4]^-$ tetrahedra.
(iii) Single heteroatoms substituted into the zeolite framework.

Each of these composite configurations is characterized by specific chemical, physical, and catalytic properties. Many approaches have been developed for the well-defined synthesis of these materials, i.e., preparation of zeolite–metal composites with uniform metal sites. In the following section, we will discuss some of the most common synthesis techniques, including ion-exchange, chemical vapor deposition, isomorphous substitution, and direct encapsulation of metal complexes.

Ion-Exchange, Chemical Vapor Deposition, Ligand Exchange. Favored for its simplicity and economic advantages, wetness/wet impregnation with solutions of metal salts is the most straightforward and the most frequently applied method to introduce transition metal centers into the zeolite crystals. In the absence of specific metal–zeolite interactions, however, impregnation leads to an uncontrolled distribution of the metal sites both inside the pores and on the external surface. Therefore, for the synthesis of truly well-defined catalysts, more

DOI: 10.1021/acs.chemmater.8b01311
Chem. Mater. 2018, 30, 3177–3198

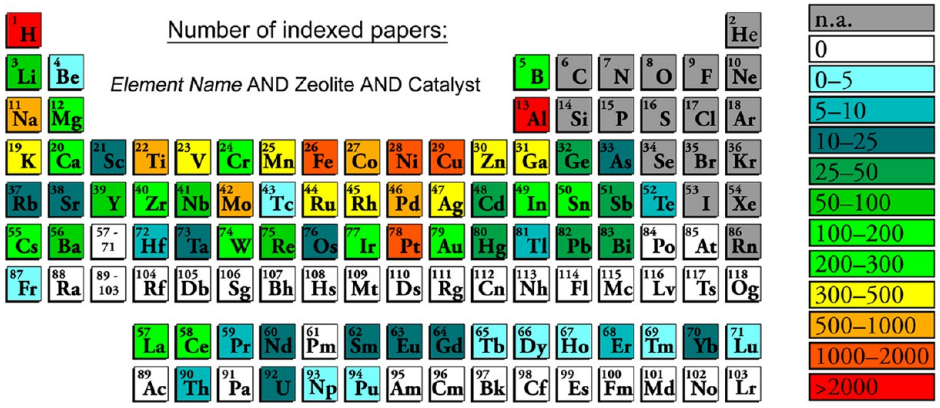

Figure 6. Number of indexed publications (average from Scopus and Web of Science), found as of November, 2017, searching for a term: "*element name* AND zeolite AND catalyst" in title, abstract, and keywords. For hydrogen, a term "proton" was used.

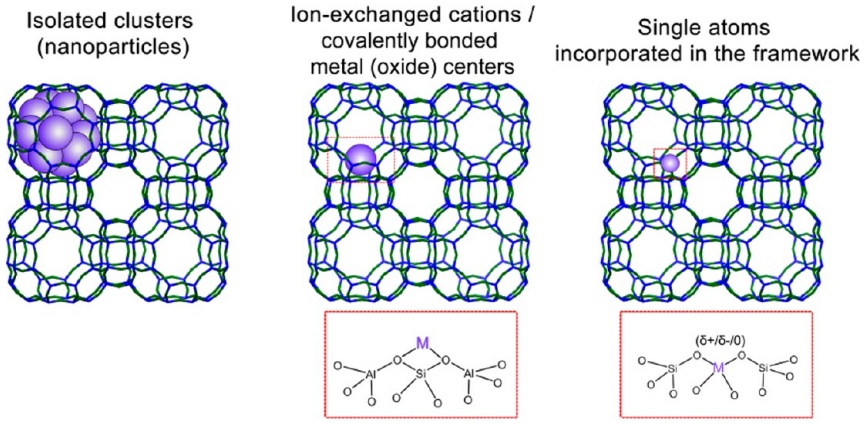

Figure 7. Possible zeolite−metal composite configurations.

sophisticated techniques are preferred. Ion-exchange is historically one of the first methods of introducing the transition-metal sites inside the zeolites pores. Typically, ion-exchange is performed in an aqueous medium using successive cycles of treatment with an excess of a targeted cation and washing. If the cation to be exchanged can be removed upon calcination (for example, H^+ as H_2O) a solid-state ion-exchange (SSIE) method can be applied as well. Typically, in the SSIE method, zeolites and metal precursor (oxides, halides, etc.) are mixed and treated at high temperature to promote the diffusion of cations inside the pores, driven by elimination of water or volatile hydrogen halides upon the ion-exchange.[56] The advantages of the SSIE method include a decreased number of steps as compared to the wet ion-exchange (since no intermediate washing or calcination are necessary), and the possibility to use cations that are difficult to ion-exchange in the aqueous medium.[57,58] Furthermore, it is much easier to control the number of the exchanged metal sites by simply varying the amount of metal precursor during the SSIE.[59] Shwan et al. recently demonstrated that the SSIE method can be greatly improved by controlling the gas-phase atmosphere during the thermal treatment step.[60] The authors were able to lower the temperature necessary for the production of several Cu-exchanged zeolites (MFI, BEA, CHA) from 700 to 800 to 250 °C by performing the treatment in a flow of nitrogen with 530 ppm of NH_3. With this approach, well-defined Cu/zeolites active for NH_3-SCR were obtained. The authors hypothesized that the formation of $[Cu(I)(NH_3)_x]^+$ species improved the mobility of the Cu phase and therefore considerably decreased the required SSIE temperature. This method can undoubtedly be applied to various zeolite frameworks and very likely to different metals as well.

Chemical vapor deposition (CVD) is a related technique that allows preparation of well-defined and often single-atom catalysts.[61] One method to perform CVD is by reacting a volatile and reactive metal precursor (chloride, carbonyl, alkyl, etc.) with a zeolite under anhydrous conditions and elevated temperatures. A stoichiometric chemical reaction between the Brønsted acid sites and reactive precursor leads to a selective deposition of metal cations. In this manner, it is possible to synthesize zeolites modified with, for example, Zn (using dimethyl zinc as precursor),[62] Sn ($SnCl_4$),[63] Ga ($Ga(CH_3)_3$),[64] Re (NH_4ReO_4),[65] and Ni ($Ni(C_5H_5)_2$).[66] Cyclopentadienyl complexes are also linked to another class of techniques that can be called ligand exchange: adsorption of metalorganic complexes onto the surface of zeolites that, upon (partial) decomposition, can migrate inside the pores, eventually forming a complex with the zeolite frameworks by exchanging or interacting with Brønsted acid sites.[67] Gates and co-workers have mastered this synthesis strategy and prepared a series of well-defined single-site and single-atom catalysts. The library includes metal (Rh,[68] Ir,[69] Au,[70] Pt,[71] etc.) single atoms and clusters of different nuclearity prepared from commercially relevant alkyl, acetylacetonate, and carbonyl precursors and stabilized by HY zeolite, MgO, or CeO_2 among others. Gates and co-workers also demonstrated a clear advantage of using

DOI: 10.1021/acs.chemmater.8b01311
Chem. Mater. 2018, 30, 3177−3198

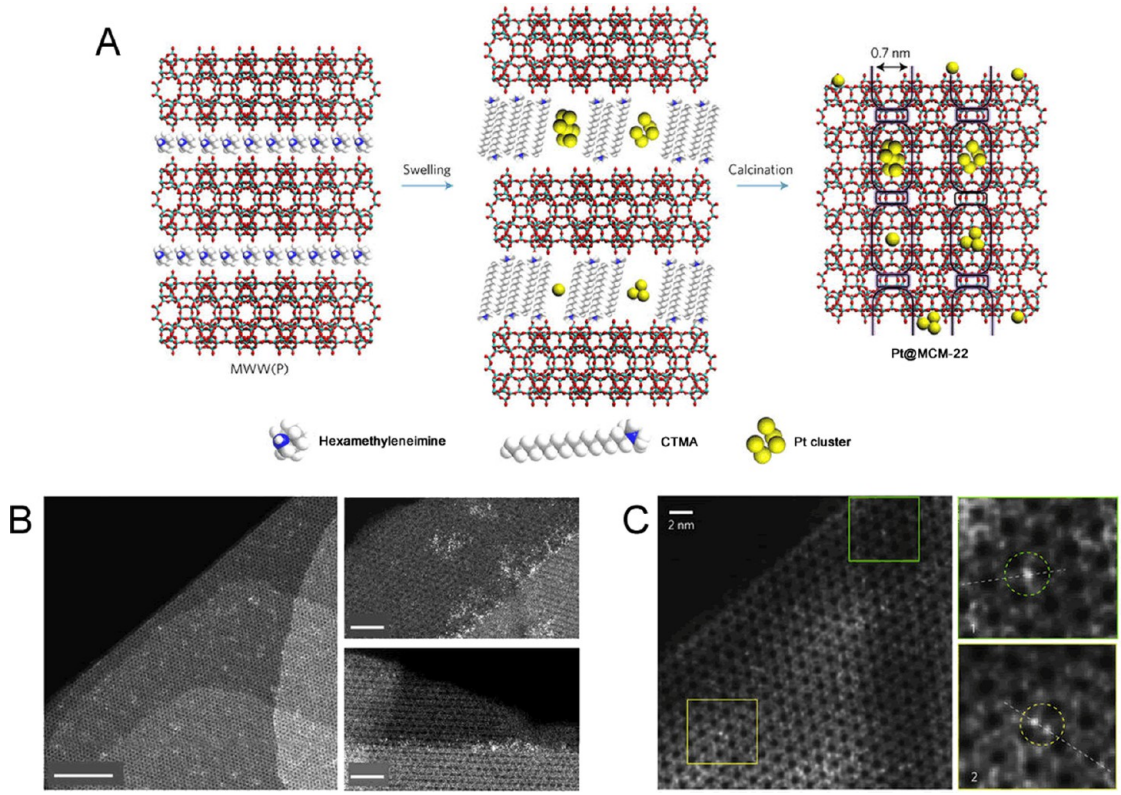

Figure 8. (A) Illustration of the preparation of Pt@MCM-22. During the swelling process of layered MWW zeolitic precursors, a solution containing sub-nanometric Pt species is added. MWW layers are expanded by the surfactant (hexadecyltrimethylammonium, CTMA+OH−), and sub-nanometric Pt species are also incorporated into the internal channels between individual MWW layers. Removing the organic agents will lead to the formation of 3D Pt@MCM-22, in which sub-nanometric Pt species are confined in the external cups on the surface or encapsulated in the supercages of MCM-22. (B) HAADF-STEM images of Pt@MCM-22. Scale bars, 20 nm (left) and 5 nm (right). (C) HAADF-HRSTEM image of Pt@MCM-22, where two zoom-ins are shown in the square regions (marked in green (#1) and yellow (#2)). In these two areas, several single atoms have been highlighted. Scale bar, 2 nm. Adapted with permission from ref 101. Copyright 2017 Macmillan Publishers Limited.

crystalline zeolite materials as supports—ligands for the stabilization of the metalorganic catalysts. The authors showed that anchoring metal complexes to the crystalline zeolite framework results in a much higher sintering resistance as compared to an amorphous silica-alumina phase and exemplified this effect by a highly stabilized $Ir(CO)_2$/HY complex formed from an $Ir(CO)_2(acac)$ precursor.[72]

Isomorphous Substitution. Unlike other metal−zeolite configurations that exclusively lead to extraframework species, the isomorphous substitution approach permits creating truly single framework metal sites. The most common heteroatom applied for the isomorphous substitution is obviously trivalent Al. Apart from charging the framework, which can then be balanced a cation, Al does not bring any special catalytic properties. Other trivalent elements such as B, Fe, Ga, and La can be also introduced into the framework, resulting in varied lattice basicity and stability.[73,74] For the purposes of this review, we will focus on tetravalent elements Ti and Sn that, upon substitution in the framework, form stable and strongly Lewis acidic single sites.

Ti-containing MFI zeolite, often referred to as TS-1, is one of the most prominent isomorphously substituted zeolite catalysts. TS-1 is a particularly efficient single-site (photo-)oxidation catalyst, active and selective, among other reactions, in epoxidation of olefins, hydroxylation of phenolics, and oxidative desulfurization.[75,76] TS-1 is usually synthesized by a bottom-up approach, i.e., direct incorporation of Ti into the zeolite framework during the synthesis, using alkoxide Ti precursors.[77]

Following TS-1, isomorphously substituted Sn-zeolites (particularly Sn-Beta) have attracted significant attention as superior catalysts for the conversion of biomass derived oxygenates into valuable chemical building blocks. The advantages of zeolite-based Lewis acid catalysts for the conversion of bioderivatives stems from the fact that, unlike conventional oil refinery, the biorefinery should deal with aqueous solutions.[78] Therefore, biorefinery catalysts must be able to withstand hydrothermal conditions and favor the selective adsorption of oxygenates over water.[79,80] High-silica zeolites, in addition to being hydrothermally stable, are intrinsically hydrophobic, and can even be nearly ultrahydrophobic upon surface modification,[81] making the high interest in Sn-Beta catalysts understandable. Due to its larger atomic diameter, it is significantly more difficult to incorporate Sn directly into the silicate framework.[82] Top-down approaches that allow faster preparation and higher achievable framework Sn content are more practical for the synthesis of highly active Sn-Beta catalysts.[83] For example, van der Graaff et al. used a method in which the dealumination of Al-Beta nanocrystals is followed by impregnation with $SnCl_4$ to occupy silanol nests formed upon dealumination. With this method, it was possible to obtain framework Sn content as high as 5 wt % in the absence of extraframework Sn species. The resulting catalysts were found to be highly active in conversion of 1,3-dihydroxyacetone to methyl lactate.[84]

Encapsulation. Ship-in-a-bottle synthesis techniques have attracted significant attention as a versatile method to create well-defined transition metal particles/clusters/ion complexes

DOI: 10.1021/acs.chemmater.8b01311
Chem. Mater. 2018, 30, 3177−3198

confined inside the zeolite pores. This direct encapsulation strategy is often advantageous because of the reduced number of synthesis steps required for the material preparation and high uniformity of the resulting metal centers. There are several approaches to the metal encapsulation. The most straightforward strategy is to stabilize the metal atoms/clusters in the form of an organometallic complex that can be mixed with a structure-directing agent (SDA). These are then added to the synthesis mixture during the hydrothermal zeolite growth. SDAs or templates are organic molecules (usually quaternary ammonium cations) that are applied to stabilize the desired zeolite topology during the hydrothermal synthesis.[85,86] In this regard, metal complexes can act as single SDA, co-SDA, or can be just confined inside the pores of growing zeolite without directing the structure.[87] One of the most important parameters during the ship-in-a-bottle synthesis is the stability of the metal complex during the zeolite synthesis, usually carried out under strongly alkaline conditions and at elevated temperatures. The in situ encapsulation method in different modifications has been applied for the synthesis of a large variety of metal−zeolite composites, including metal complexes confined in zeolites, metal oxide, and metal (sub-)nanoparticles (after decomposition and reduction of the precursor complex, respectively). Notably, metal clusters, prepared from ethylene diamine or ammonia precursors and encapsulated in the cavities of zeolites, such as (Pt, Pd, Rh, Ir, Re, Ag, Au and Co_3O_4)@LTA,[88−90] Pd@silicalite-1,[91] and (Pt, Pd, Ru, Rh)/(SOD, GIS)[92] have been reported. Recently, preparation of a bimetallic (Ni,Co)-Pd@silicalite-1 catalyst, from the respective Ni and Pd ethylenediamine complexes, with greatly improved activity in selective formic acid decomposition to CO_2 and H_2, has been reported as well.[93] Apart from using nitrogen-containing ligands, mercaptosilanes such as (3-mercaptopropyl)trimethoxysilane are suitable molecules for the stabilization of metals during the hydrothermal zeolite synthesis. Strong bonding of the mercapto-group to transition metals and copolymerization of the alkoxysilane group with the zeolite organosilane precursor ensures effective encapsulation of highly dispersed mono- and bimetallic[94] metal centers.[95,96]

Recrystallization of the zeolite in the presence of a metal precursor and related techniques present another approach to encapsulate nanoparticles and even single atoms inside the zeolite.[97−99] For instance, Liu et al. applied a process of 2D-to-3D transformation of MCM-22 (MWW) zeolite[100] to confine Pt sub-nanoparticles inside the pores. Two-dimensional MWW layers can be prepared by using surfactant molecules. Lie et al. mixed the 2D MWW precursor with a dispersion of sub-nanometer Pt particles in DMF. Once the surfactant was removed by calcination, the 2D MWW precursor transformed into a 3D MCM-22 structure with the Pt species encapsulated inside (Figure 8). By using high-resolution electron microscopy, X-ray absorption, and fluorescence emission spectroscopy, the authors found that the obtained Pt@MCM-22 catalyst contained Pt as sub-nanoclusters (ca. 80%) and single atoms (20%). Eventually, Pt@MCM-22 displayed a high activity in shape-selective hydrogenation of light olefins and a remarkable stability during oxidation−reduction cycling at 650 °C.[101]

Hollow zeolites are an emerging type of structured zeolite materials with improved diffusion properties, achieved by reducing the thickness of the microporous wall.[102] In addition to enhanced catalytic efficiency, hollow zeolites can be used as nanocontainers to confine and stabilize well-defined small metal nanoparticles.[103] Recently, Tuel and co-workers developed and optimized a synthesis strategy to prepare Co, Ni, Cu, Ag, Pt, and Au[104−107] nanoparticles confined in hollow ZSM-5 and silicalite-1 crystals by impregnation of parent microporous zeolite crystals with the solution of a metal salt, followed by desilication−recrystallization with TPAOH solution, calcination, and reduction. The resulting yolk−shell materials were defined by a very narrow and controllable metal particle size distribution (achieved by varying the concentration of the metal salt solution), complete confinement of nanoparticles inside the zeolite shell, and, consequently, high resistance to sintering even upon high-temperature reductive treatment. Seemingly, the only drawback of this simple and scalable method is a difficulty to achieve a high metal loading in the final catalyst.

Overall, further development of encapsulation techniques will certainly lead to an expansion of the library of metal as well as metal oxide, carbide,[108] sulfide,[109] etc., catalysts that can be confined inside the zeolite pores, for performing various catalytic reactions in a shape-selective manner.

Tuning the Zeolite Properties. Numerous modification techniques have been developed to tune the chemical, textural, and structural properties of the zeolite-based catalysts. Here, we will briefly discuss recent developments in the pre- and postsynthesis modifications of zeolitic materials.

Controlled Distribution of T Atoms. Controlling the distribution of T atoms within the framework is a fine approach to adjust the coordination and therefore the properties of the transition metal sites inside high-silica zeolite pores. Several promising methods to regulate the distribution of T atoms (primarily Al) within the framework during the hydrothermal synthesis and to determine this distribution have been developed.[110] The distribution of Al atoms can be tuned from two perspectives: selective occupation of certain crystallographic sites or positions within the crystal (in cavities, intersections, channels, or pockets), and the positioning of Al atoms with respect to other Al atoms.

Distribution of Al atoms within the framework can be controlled by varying template molecules or mixing different templates. Since isomorphous substitution of Al is accompanied by the positive charging of the framework, an inorganic (Na^+, K^+, etc.) or organic (SDA) cation has to be present during the synthesis to ensure the Al incorporation. This phenomenon gives rise to several elegant synthetic strategies of directing the Al atoms. For instance, the most studied framework MFI is typically synthesized in the presence of tetrapropylammonium (TPA^+). This bulky cation does not fit the MFI channels and directs the growth of the structure by residing in the spacious intersection of straight and sinusoidal channels. Therefore, if TPA^+ is the only cation present during the synthesis of MFI, the Al is preferentially introduced in the intersections. If small Na^+ cations are added to TPA^+, Al is distributed more or less evenly throughout the framework.[111] However, if TPA^+ cations are replaced by pentaerythritol (an uncharged tetraol molecule which is geometrically similar to TPA^+) and Na^+ is added, Al preferentially sits inside the channels.[112] At the same chemical composition and pore topology, the ZSM-5 samples with preferential Al location display significantly different catalytic properties, allowing the design of improved catalysts.[113] Conceptually similar approaches were applied to prepare such zeolites as CHA,[114] FER,[115] and RTH[116] with preferential Al distribution.

Generally, the Löwenstein rule prohibits the formation of Al-O-Al linkages within the zeolite framework, although it was proposed that some violations of this rule are theoretically

DOI: 10.1021/acs.chemmater.8b01311
Chem. Mater. 2018, 30, 3177−3198

possible.[117] Even without breaking the Löwenstein rule, the presence of Al in Al-O-Si-O-Al and Al-O-(Si-O)$_{n=2,3}$-Al (so-called Al pairs), or in Al-O-(Si-O)$_n$-Al (n > 3, isolated Al atoms) fragments (Figure 9), is critical for the catalytic properties[118] and particularly for the stabilization of transition metal cations.

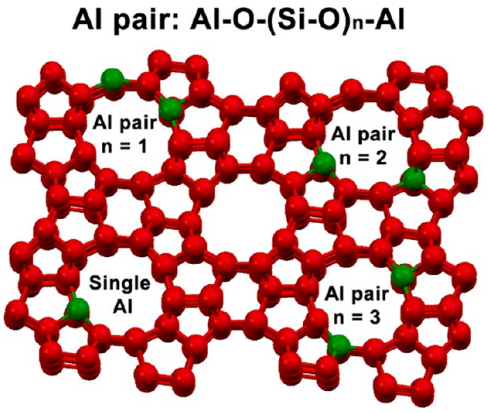

Figure 9. Some possible configurations of Al distribution within MFI framework.

In short, a pair of Al atoms in close proximity to each other are able to balance the charge of a divalent (oxo-)cation, while a single or isolated Al atoms cannot. Recently, in a series of papers, Wichterlová and co-workers reported a way to control the pair/isolated Al distribution. The authors found that, by enhancing the polarization of TPA^+ cations with smaller counteranions (Cl^- instead of NO^{3-}), or by using Al precursors giving rise to dimeric Al species, it is possible to maximize the number of Al pairs. Alternatively, at high concentrations of Na^+ and in the presence of reactive Al-oxo monomers, the formation of single Al sites was predominantly observed.[119,120]

The possibility to control the distribution of Al atoms is particularly important for the synthesis of well-defined transition metal centers. Generally, Al pairs provide stronger stabilization for polyvalent metal and metal-oxo cations than isolated Al sites. The framework incorporation of Al as pairs or isolated sites was recently utilized for the preparation and characterization of distinct reactive transition metal sites in Mo/ZSM-5,[121] Co/Beta,[122] and Cu/SSZ-13[123] systems.

Core–Shell Structuring. The external surface of zeolite crystals usually contains the same functional groups as the pore interior—most notably Brønsted acid sites. Therefore, the activity of a zeolite's external surface is not negligible. Since the shape selectivity does not play a role outside of the pores, this activity often leads to the unselective reactions, decreasing the overall efficiency of a catalytic process.[124] Core–shell structuring combining an active zeolite core and an inert shell is a smart solution to this problem.[125] As an example, Ghorbanpour et al. recently reported a method to prepare an ultrathin epitaxially grown shell of silicalite-1 (pure-silica MFI) over ZSM-5 nanocrystals.[126] The authors determined the epitaxial growth rate and were able to grow a high-quality silicalite-1 film as thin as a few nanometers on the surface of ZSM-5. As a result, the obtained ZSM-5@silicalite-1 material had a completely inactive external surface without compromising the intrinsic microporous activity. This result was evidenced by an unaffected rate of acidic acid ketonization over the composite catalyst (acetic acid is a small molecule that can diffuse through the MFI pores), and nearly zero activity in cracking of large triisopropylbenzene molecules (Figure 10). Core–shell structures comprising two different zeolite top-

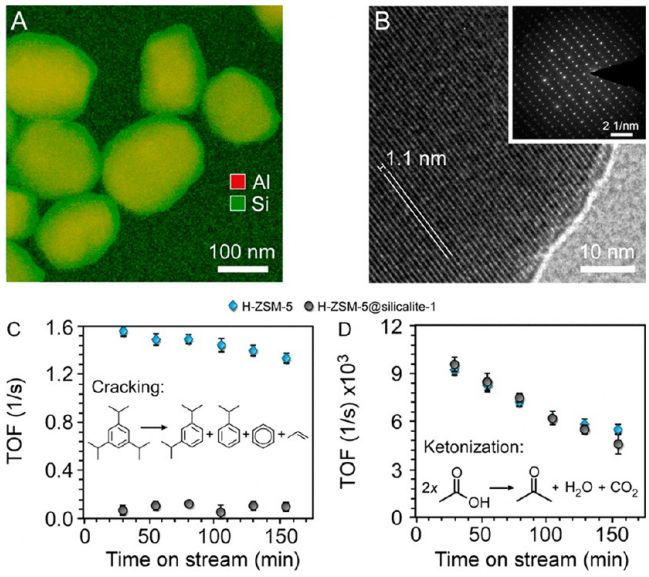

Figure 10. (A) Superimposed EFTEM mapping of annealed ZSM-5@silicalite-1 crystals prepared with a 10 nm silicalite-1 shell. The elements are color coded: Al (red) and Si (green). (B) HRTEM image of a core–shell crystal reveals the presence of lattice fringes that extend from the exterior to the interior of the particle without any discontinuity. The orientation of fringes (1.1 nm periodicity) is highlighted by the white lines. Gas-phase turnover frequency (TOF) in a flow reactor of (C) 1,3,5-triisopropylbenzene and (D) acetic acid over H-ZSM-5@silicalite-1 prepared with a 10 nm silicalite-1 shell, as well as the H-ZSM-5 core. The reactions were performed at 1 atm after pretreating the catalyst in He flow at 300 °C for 1 h to remove physisorbed water from the catalyst surface. Cracking of triisopropylbenzene (C) was done at 400 °C and ketonization of acetic acid (D) was done at 320 °C. Adapted with permission from ref 126. Copyright 2015 American Chemical Society.

ologies that are promising materials for shape-selective catalysis and adsorption applications have also been reported.[127] With respect to transition metals, encapsulation of Fe/ZSM-5[128] and Mo/ZSM-5[129] with a silicalite-1 film was shown to result in improved NH_3-SCR and MDA performance, respectively, explained by the decreased external surface activity.

Hierarchical Structuring. Diffusion limitations often complicate the conversion of organic molecules, with the severity of these limitations more pronounced for bulky ones. Hierarchical structuring, i.e., creating zeolite materials having more than one level of porosity, is a conventional approach to enhance the diffusion and therefore catalytic properties of zeolite materials.[130] Remarkable progress has been achieved in the synthesis and understanding of hierarchical zeolites during the last two decades.[131] Broadly, top-down (creating secondary mesoporous pore network within microporous zeolites) methods such as desilication or dealumination and bottom-up approaches (growing micro/mesoporous zeolites using mesoporogen template agents) can be distinguished.[132] Although the top-down methods are relatively simple and can be performed by acid leaching (to remove Al atoms), alkaline leaching (to remove Si atoms), or even by heavy ion bombardment, followed by hydrofluoric acid treatment to remove both,[133] these strategies can damage the zeolite crystallinity and therefore the microporosity.[134] Since the active sites for the

DOI: 10.1021/acs.chemmater.8b01311
Chem. Mater. 2018, 30, 3177–3198

majority of zeolite-catalyzed reactions should reside inside the micropores, the loss of microporosity is highly undesirable. Hierarchy factor, proposed by Pérez-Ramírez et al., is a particularly useful concept in the field of hierarchical zeolites.[135,136] Hierarchy factor is an indicator of the mesoporous area enhancement ($S_{mesopores}$) and corresponding decrease of the microporous volume ($V_{micropores}$) for a given hierarchical zeolite, as outlined by the following formula:

$$\text{Hierarchy Factor} = \frac{V_{micropores}}{V_{total}} \times \frac{S_{mesopores}}{S_{total}}$$

A zeolite material with a high hierarchy factor would have a small decrease of microporosity at high mesoporous volume and thus advantageous catalytic properties. A fine illustration of this concept is a mild and controllable desilication method developed by Pérez-Ramírez et al. To enhance the control during the desilication, the authors used mixtures of NaOH with quaternary ammonium cations (TPA^+ or TBA^+) that stabilize the zeolite framework during the alkaline leaching. As a result, it was possible to control the hierarchy factor of the materials by simply varying the TPA^+/OH^- ratio during the desilication. Eventually, a linear correlation was found between the hierarchy factor of obtained hierarchical ZSM-5 catalysts and their productivity in liquid phase alkylation of benzene with ethylene.[135]

Bottom-up or template-assisted approaches are synthetic techniques that provide a way of fabricating mesoporous zeolite materials with predesigned textural properties. Solid and surfactant templating can be distinguished. Solid templating involves polymer beads or carbon nanoparticles/nanotubes that are added during the zeolite synthesis and then removed by combustion.[137] Surfactant templating with bulky amphiphilic ammonium salts[138] has attracted significant attention after breakthrough works of Ryoo and co-workers. They among other materials developed the controllable synthesis of various mesoporous zeolite topologies using [3-(trimethoxysilyl)-propyl]hexadecyldimethylammonium (TPHAC),[139] single-unit-cell nanosheets of zeolite MFI in the presence of a diquaternary ammonium surfactant $C_{22\text{-}6\text{-}6}$ (Figure 11),[140] and hexagonally ordered hierarchical MFI architectures.[141]

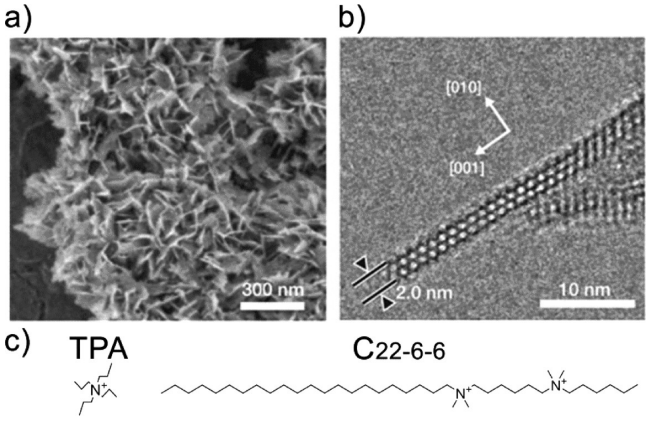

Figure 11. SEM (a) and cross-sectional TEM (b) images of the of the unilamellar MFI nanosheet with unit cell thickness along the MFI *b*-axis of b = 1.9738 nm; (c) structure of tetrapropylammonium cation typically used for the synthesis of MFI zeolites and mesoporogen $C_{22\text{-}6\text{-}6}$ applied by Ryoo and co-workers. Adapted with permission from ref 140. Copyright 2009 Macmillan Publishers Limited.

Subsequent investigations greatly expanded the library of zeolite topologies that can be prepared hierarchically, using the surfactant templating approach,[142−146] led to a discovery of a series of low-cost amphiphilic templates,[147−150] and even organic-free routes for the direct bottom-up synthesis of hierarchical zeolites were reported.[151,152] The possibility to rationally design the amphiphilic mesoporogens was recently outlined by Zhu et al., who studied the early stages of MFI nanosheet synthesis by operando small-angle X-ray scattering, complementary characterization techniques, and molecular modeling.[153] The authors found that the meso-order is established at the very beginning of synthesis and that amphiphilic SDA stabilizes pre-zeolitic species via a molecular-recognition-type mechanism, followed by the micro-ordering into zeolite nanosheets. It was also shown that the rational fine-tuning of the ammonium headgroup allows synthesis of different zeolite topologies (namely, MFI and MEL) and aspect ratios (nanosheets or needles).

Hierarchically structured zeolites offer a versatile playground for the development of well-defined transition metal centers. First of all, the high surface area of these materials allows preparing catalysts with higher metal loading, while the small size of the microporous domains greatly improves the diffusion properties. A proper balance between microporous and external (mesoporous) areas should be usually ensured to fully utilize the shape-selective properties of zeolites without nonselective conversion on the external surface.[154]

■ ADVANCED CHARACTERIZATION METHODS IN SINGLE-SITE ZEOLITE CATALYSIS

Characterization of ultra-dispersed metal sites confined in zeolites is by no means an easy task. Most often, to fully understand the structural features and catalytic properties of these materials, a combination of several techniques should be applied.[155] For instance, Gates and co-workers developed a strategy for the characterization of atomically dispersed metal sites, combining high-angle annular dark-field aberration-corrected scanning transmission electron microscopy (HAADF-STEM), extended X-ray absorption fine structure (EXAFS) spectroscopy, and Fourier transform infrared spectroscopy (FTIR) with CO as probe molecules, followed by full-width half-maximum analysis of the observed carbonyl bands.[156] This set of complementary techniques allows an unequivocal characterization of single-atom and cluster metal species.[157] Further, after a remarkable progress in the development of operando techniques has been achieved within the last few decades,[158] such methods are becoming indispensable in catalysis research.[159,160] Table 2 lists typical physical-chemical techniques applied for the characterization of metal−zeolite composites; references to the respective review papers and book chapters are also provided. In the next sections, we will discuss the applicability of some of the most relevant techniques to the highly dispersed metal−zeolite catalysts and provide some illustrative examples of recently reported operando spectroscopy studies.

Microscopy. Naturally, microscopy as a visualizing technique is appealing for the characterization of composite catalytic materials. While transmission electron microscopy (TEM) is a routine technique for studying typical heterogeneous catalysts containing metal nanoparticles with sizes ranging from 1 to 100 nm, for the characterization of sub-nanometer metal sites confined inside the zeolite pores, the resolution of TEM is often insufficient.[184] For the reliable analysis of sub-nanometer features with atomic resolution, the high-angle annular dark-field detection scanning transmission electron microscopy (HAADF-STEM) technique is usually a method of choice. STEM is based on scanning the specimen across with the electron beam. In comparison with conventional TEM, this method results in a stronger interaction of the electrons with the sample and therefore more types of signals, detectable with high spatial resolution, being produced.

DOI: 10.1021/acs.chemmater.8b01311
Chem. Mater. 2018, 30, 3177−3198

Table 2. Selected Physical-Chemical Methods Applied for the Characterization of Transition Metal−Zeolite Catalysts

technique	information about the metal centers or zeolite framework	ref
atom probe tomography	spatial distribution of elements	161
computational modeling	structure and stability of metal centers, activity mechanism	162, 163
electron microscopy (TEM, SEM, STEM)	particle size distribution, homogeneity of the metal centers	164
electron paramagnetic resonance (EPR) spectroscopy	structure of paramagnetic metal centers	165, 166
Mossbauer spectroscopy	structure of Mossbauer-active metal centers	167
nuclear magnetic resonance (NMR) spectroscopy	structure of NMR-active metal centers, framework acidity	168−170
physisorption (Ar, N_2, CO_2)	textural properties of the framework	171, 172
temperature-programmed techniques (TPD, TPR, TPO, TPSR)-MS	structure, stabilization degree, and reactivity of metal centers	173
UV−vis spectroscopy	structure and location of metal centers	174
vibrational (probe) spectroscopy (FTIR, Raman)	structure of metal centers, framework acidity	175−177
X-ray absorption/X-ray emission spectroscopy (XAS/XES), X-ray photoelectron spectroscopy (XPS)	structure, oxidation state, and external/internal distribution of metal centers	178−181
X-ray diffraction (XRD, XRD-PDF), small-angle X-ray scattering (SAXS)	crystalline phase purity, structure, size distribution, and geometry of metal clusters	182, 183

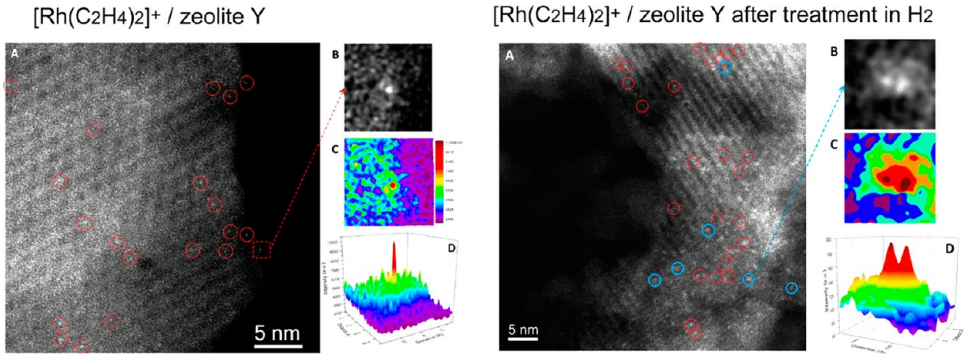

Figure 12. Aberration-corrected HAADF-STEM characterization of $[Rh(C_2H_4)_2]^+$ complexes on zeolite HY, before (left) and after (right) treatment in H_2/He flow at 373 °C for 4 min. (A) HAADF-STEM images. (B) Magnified views of corresponding areas in (A), with the intensity surface plots shown in (C) and the three-dimensional intensity surface plots shown in (D). Bright features encircled on the left panel are examples of individual Rh atoms and on the right panel of both single Rh atoms (red circles) or Rh dimers (blue circles). Adapted with permission from ref 187. Copyright 2016 American Chemical Society.

These signals include characteristic X-rays, useful for reconstructing the energy dispersive X-ray (EDX) elemental maps, and inelastically scattered electrons allow for electron energy loss spectroscopy (EELS) analysis.[185] The most important signal comes from elastically backscattered electrons, which are used to reconstruct the dark-field atomic resolution image of the sample, by applying an HAADF detector. Since electron scattering efficiency depends on the element atomic number, the resulting STEM images are characterized by a Z-contrast.[186] This property is particularly advantageous for studying atoms/clusters of heavy metals dispersed within the zeolite crystals composed of light elements Si, Al, and O.

This concept is illustrated by a study of $[Rh(C_2H_4)_2]^+$ clusters, confined inside the pores of HY zeolite, by Yang et al.[187] Careful HAADF-STEM analysis of fresh catalysts and those after a reductive treatment of different duration allowed the authors to track the dimer intermediates during the sintering of the Rh phase (Figure 12). Furthermore, the authors supported the STEM results by an X-ray adsorption analysis and found a clear correlation between the dispersion of the active phase and its catalytic performance in ethylene dimerization. HAADF-STEM is a truly versatile tool for the analysis of sub-nm systems. However, because zeolites can be damaged relatively easily by the high-energy electron beam during measurements, it requires the presence of heavier metals that are easier to detect in the material. This somewhat limits the applicability of the characterization technique.[188]

A nondestructive microscopy tool for metal−zeolite composites emerging in catalytic studies is fluorescence microscopy. Although the intrinsic resolution of fluorescence microscopy is limited by the half of visible light wavelength (ca. 200 nm), it is possible to break this limit by applying the so-called super-resolution fluorescence microscopy.[189] This stochastic approach is particularly useful for studying catalysts and is suitable for operando studies.[190] The stochastic super-resolution fluorescence microscopy is based on collecting transient fluorescent signals with high-temporal resolution. In catalysis, it can be performed by recording single catalytic turnovers during conversion of fluorogenic substrates, where time-resolved turnovers allow for the determination of the spatial distribution of active sites within the catalyst particles.[191] One method that found an aplication for zeolite-based materials is nanometer accuracy by stochastic chemical reactions (NASCA) microscopy, developed by Roeffaers and co-workers.[192] This method was applied to study the distribution of Brønsted acid sites, by recording catalytic fluorescent events, occurring upon protonation and oligomerization of furfuryl alcohol[193] or substituted styrenes.[194] NASCA microscopy is a versatile tool to visualize the microstructure of zeolite catalysts, especially hierarchically structured ones.[195] For example, Figure 13 demonstrates results of Kubarev et al., who studied mesoporous mordenite samples by NASCA microscopy using furfurol and furfurol oligomerization as a probe molecule and a fluorescent probe reaction, respectively.[196] Combining NASCA results with SEM, the authors were able to determine the spatial distribution of non-zeolitic pores with high resolution and concluded that the diffusivity of reagent molecules is only enhanced in the micropores, which are located in close proximity to the meso/macropores. Therefore, to achieve the optimal reactivity, the size of microporous clusters should be carefully controlled.

Currently, single molecule fluorescence microscopy studies mainly focus on the distribution and relative activity of Brønsted acid sites. We envisage that, with further development of the technique, suitable probe molecules and probe reactions will be identified to extend the

DOI: 10.1021/acs.chemmater.8b01311
Chem. Mater. 2018, 30, 3177−3198

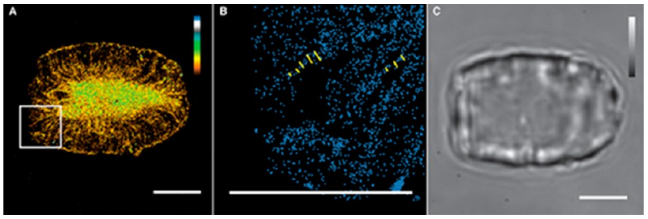

Figure 13. Optical microscopy investigation of furfuryl alcohol conversion inside a hierarchical mordenite crystal. Scale bars: 3 μm. (A) NASCA reactivity map obtained for 50 × 50 × 800 nm^3 voxels (*xyz*) for the duration of 500 s. False color scale shows the observed relative reaction rate; white rectangle indicates area enlarged in panel (B). (B) Magnification showing the scatter plot with locations of individual reaction events; yellow lines indicate distances taken for region width estimation. (C) Corresponding bright-field optical transmission image. Adapted with permission from ref 196. Copyright 2015 Wiley.

applicability of this powerful method to the transition metal sites as well.

Atom Probe Tomography. Unique information that can be obtained by atom probe tomography (APT) has made this technique an extremely promising tool for material studies. The detection principle of modern APT systems is based on a combination of time-of-flight (TOF) mass spectrometry and a point projection microscope.[197] A sample processed to a shape of a thin needle (ca. 100 nm) by focused ion beam (FIB) milling[198] is exposed to cryogenic temperature and high vacuum, and then a voltage from a local electrode is applied. When the voltage is high enough, atoms from the surface of the sample are field evaporated. By using short voltage pulses (or laser pulses), it is possible to set the start time of any evaporated ion. This combination of data provides full 3D element distribution maps of the sample with outstanding spatial (0.1−1 nm) and mass resolutions.[199] Although APT is still a relatively rare method and has some applicability and analysis limitations,[200] it has already established itself as one of the most powerful and promising characterization techniques in material science in general, as well as for specifically investigating the zeolite-based catalysts.[201,202] Figure 14 demonstrates recent results of Schmidt et al., who followed the deactivation of Cu/SSZ-13 and Cu/ZSM-5 deNO_x catalysts with APT.[203] The authors were able to visualize the distribution of Cu species in fresh and aged catalysts and identified these species as dispersed Cu sites, larger Cu-oxo clusters, and $CuAl_2O_4$ spinel. Importantly, the authors could understand the higher catalytic stability of Cu/SSZ-13 catalysts as compared to Cu/ZSM-5. In the latter, severe agglomeration of the Cu phase, dealumination, and formation of $CuAl_2O_4$ were observed on the atomic level. These phenomena resulted in a structural degradation and eventually in a significant decrease of the catalytic activity.

X-ray Methods. X-ray diffraction (XRD) and X-ray photoelectron spectroscopy (XPS) have become routine laboratory tools in material science and catalysis over the last decades. However, the characterization of highly dispersed metal sites in zeolites usually requires synchrotron-based X-ray techniques. In this regard, X-ray absorption (XAS) is probably the most commonly applied method that has been particularly useful for operando studies under actual reaction conditions.[204] XAS is an element-selective spectroscopy technique that is used to record the absorption spectra occurring during core-electron excitation, as a function of photon energy. XAS can be applied to systems in any state of matter (even in plasma)[205] and nearly any concentration from ppm levels (in fluorescence mode) to tenth of percent (in transmission mode).[206] During XAS studies, typically two techniques are combined: XANES (X-ray absorption near edge structure) and EXAFS (extended X-ray absorption fine structure). XANES concerns the region right before and 0.05−0.1 keV after the absorption edge and provides information about the oxidation state of the studied element and its local symmetry. Usually, XANES spectra of the studied materials are compared with the reference spectra to

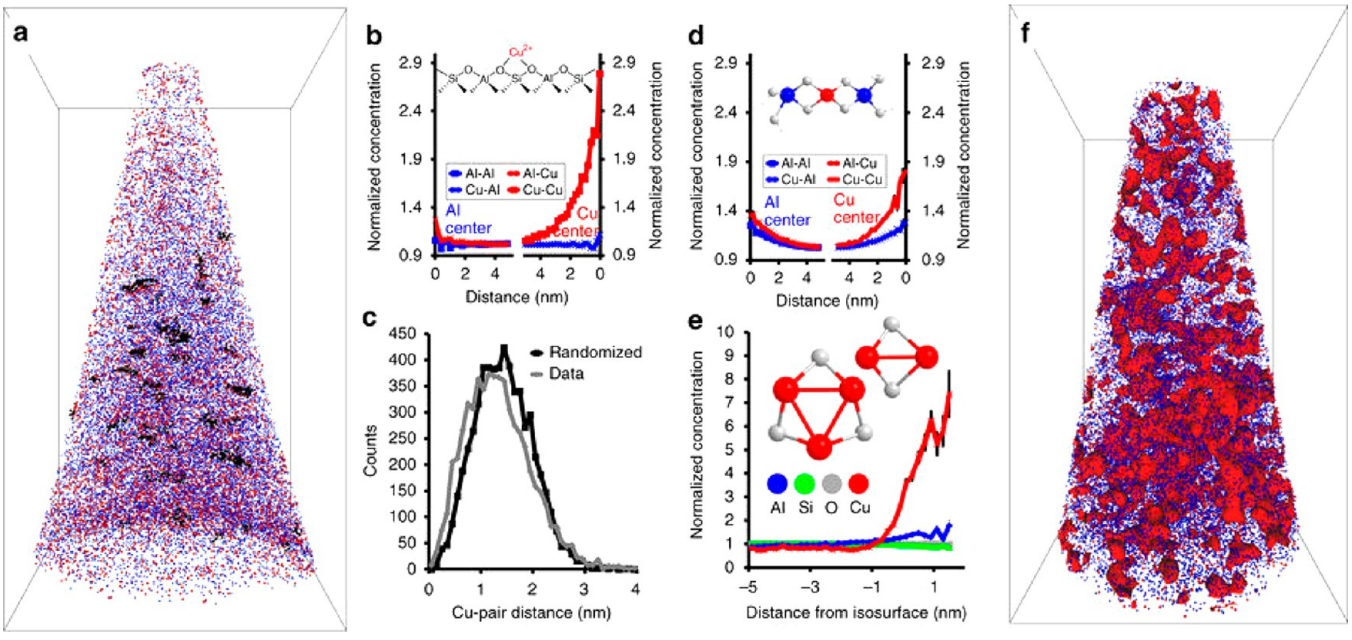

Figure 14. (a) Reconstructed needle of fresh Cu-SSZ-13 with Cu (red) and Al (blue) ions shown with Cu clusters overlaid in black. Bonding box dimensions are 63 × 67 × 115 nm^3. (b) Radial distribution functions (RDFs) in fresh Cu-SSZ-13 for Al and Cu centers. Al−Cu affinity is indicated, which would be expected due to Cu exchanging onto paired Al sites, as indicated in the schematic. (c) Nearest neighbor distribution for fresh Cu-SSZ-13 for Cu showing a significant deviation from a random distribution and indicating the presence of Cu clusters. (d) RDFs in aged Cu-SSZ-13 for Al and Cu centers. Strong affinities are indicated between all species, pointing to the migration and aggregation of Cu with aging, and a Cu aluminate species is shown, though it was not quantitatively identified. (e) Normalized compositional histogram across 1.4% Cu isoconcentration surfaces in aged Cu-SSZ-13, with potential CuO species shown. (f) Reconstructed needle of aged Cu-SSZ-13 with 1.4% Cu isoconcentration surfaces shown. Bonding box dimensions are 49 × 52 × 90 nm^3. Reproduced with permission from ref 203. Copyright 2017 Macmillan Publishers Limited.

DOI: 10.1021/acs.chemmater.8b01311
Chem. Mater. 2018, 30, 3177−3198

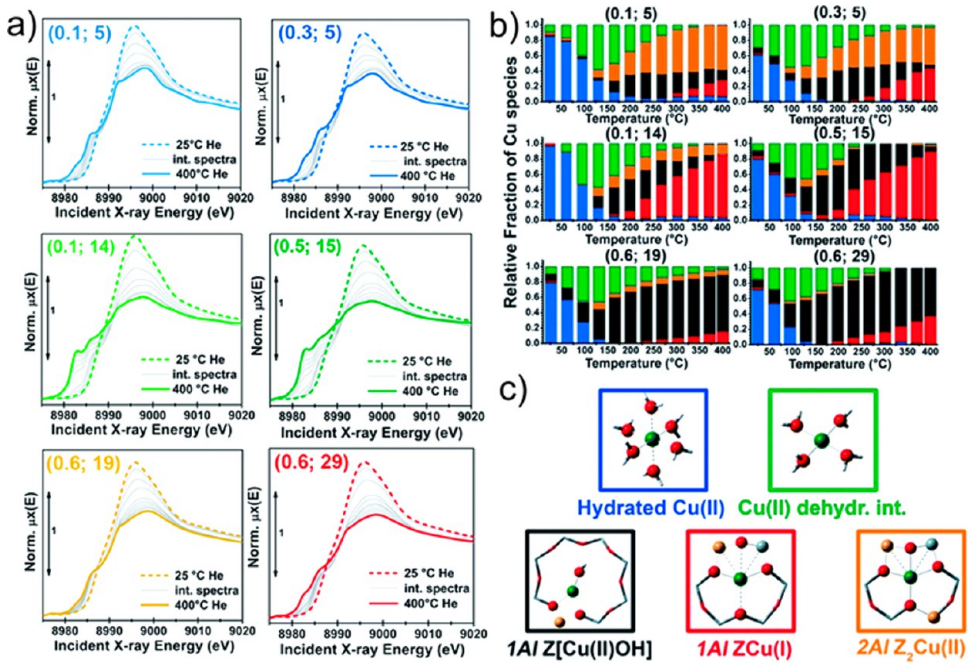

Figure 15. (a) In situ XANES of Cu-CHA catalysts with different compositions (different samples are denoted with (Cu/Al; Si/Al) labels) during dehydration under He flow from 25 to 400 °C, heating rate 5 °C min^{-1}. (b) Temperature-dependent abundance of pure Cu species in each of the catalysts as derived from multivariate curve reconstruction based on alternating least-squares (MCR-ALS) analysis of global temperature-dependent XANES data set collected for six Cu-CHA samples. (c) Proposed assignment of the five pure components to specific Cu species/sites formed in the Cu-CHA catalyst as a function of composition and activation temperature, using the same color code as in part (b). Blue (PC1): mobile Cu(II)-aquo-complexes $[Cu(II)(H_2O)_n]^{2+}/[Cu(II)(H_2O)_{n-1}(OH)]^+$ with $n = 6$; green (PC5): Cu(II) dehydration intermediate, possibly represented by mobile $[Cu(II)(H_2O)_n]^{2+}/[Cu(II)(H_2O)_{n-1}(OH)]^+$complexes with $n = 4$; black (PC3): 1Al Z[Cu(II)OH] sites in their oxidized form; red (PC2): 1Al ZCu(I) sites in their reduced form, resulting from self-reduction of 1Al Z[Cu(II)OH] species; orange (PC4): 2Al $Z_2Cu(II)$ sites. Atom color code: Cu: green; H: white; O: red; Si: gray; Al: yellow. Adapted with permission from ref 214. Copyright 2017 The Royal Society of Chemistry.

fingerprint the spectral features with some known structural properties.[207] In turn, EXAFS deals with oscillations in the high-energy part of the absorption spectra that mainly originate from the backscattering of the emitted low-wavelength photoelectrons by neighboring atoms. Analysis of the oscillation patterns provides structural details (chemical speciation, coordination numbers, and bond distances) of the several coordination shells around the atom of interest.[208] It is important to note that, since the thermal disorder in solids increases as a function of temperature, recording the high-quality EXAFS spectra often requires the use of cryostats.[209] Unlike EXAFS, the quality of XANES data is hardly influenced by temperature. Moreover, XANES spectra can be recorded extremely fast (as fast as tens of ps);[210] thus XANES is a technique of choice for operando catalytic studies.[211] Notable related techniques, based on recording emission spectra of filling the core hole formed after X-ray absorption, include X-ray emission spectroscopy (XES), resonant XES, and resonant inelastic X-ray scattering (RIXS). These techniques are highly sensitive tools for studying the electronic structure of metal sites.[212,213]

Overall, the possibility to perform operando X-ray absorption spectroscopy allows for detailed characterization of the metal centers before the reaction, during the catalyst activation, at steady-state performance, and after deactivation, all in a single experiment. A recent example of this versatility comes from a work of Martini et al., who derived a complete structural characterization of a Cu/CHA system and its dynamics by multivariate analysis of operando XANES data collected at different temperatures and with varying catalyst composition, combined with EXAFS fitting, DFT modeling, and N_2-FTIR spectroscopy.[214] Cu/CHA is a promising deNO_x catalyst, but the speciation and especially the evolution of Cu sites under the reaction conditions are not completely understood.[215,216] Martini et al. thoroughly analyzed six Cu/CHA catalysts with different Cu/Al and Si/Al ratios by operando XANES (Figure 15). In the absence of reference spectra necessary to perform the linear combination fitting of the XANES data, the authors identified a number of pure Cu components by principal component analysis (PCA), and extracted the theoretical reference spectra of these components by multivariate analysis. As a result, by using this method of multivariate curve reconstruction based on alternating least-squares (MCR-ALS), the authors were able to fully follow the dynamics of Cu species (reducibility and coordination) in the Cu/CHA system as a function of temperature and chemical composition. Having analyzed these dynamics, the authors concluded that the Si/Al ratio is a key parameter influencing the reducibility of the active Cu species in a rather complex manner. Higher Si/Al is favorable for the formation of redox-active 1Al Cu sites (Z[Cu(II)OH]); however, the self-reduction process was found to be facilitated by acid sites and thus lower Si/Al ratio enhances the rate of the self-reduction. Overall, the MCR-ALS method, applied for the analysis of such complex operando XAS data set, allowed the authors to gain an unprecedented insight into the dynamics of the Cu/CHA system and can undoubtedly be applied to other composites.

Nuclear Magnetic Resonance (NMR) Spectroscopy. The extremely high resolution of the chemical surrounding of a nucleus (element) of interest makes magic angle spinning (MAS) solid-state NMR a powerful characterization tool for heterogeneous catalysts.[217] As with every characterization technique, MAS NMR has certain drawbacks. First, NMR often suffers from low sensitivity, caused by generally low polarization of nuclear spins. Second, the element of interest should contain NMR-active isotopes, i.e., those with nonzero nuclear spin. For instance, ^1H (natural abundance 99.98%) and ^{27}Al (100%) isotopes are abundant and collecting NMR spectra of these elements is rather straightforward; as a result, NMR-derived properties of Brønsted acidic zeolites are very well-understood. In the case of Si, the situation is already quite different, as the main isotope ^{28}Si (92.2%) is NMR-silent and recording ^{29}Si (4.7%) MAS NMR spectra requires much longer acquisition times. One possible solution to this problem is to use isotopically enriched chemicals for the preparation of samples.

DOI: 10.1021/acs.chemmater.8b01311
Chem. Mater. 2018, 30, 3177−3198

However, the price of such chemicals makes their use unfeasible for typical R&D applications.

An emerging technique of dynamic nuclear polarization (DNP) can enhance the NMR sensitivity by several orders of magnitude without using enriched compounds by transferring the spin polarization of microwave-irradiated unpaired electrons, to the analyzed nucleus. In other words, DNP-NMR makes use of the electron paramagnetic resonance effect to enhance the nuclear magnetic resonance efficiency.[218] Although the paramagnetic centers (if present) of a sample itself can be used for DNP, most commonly external organic radicals or biradicals (e.g., TOTAPOL) are premixed to the sample.[219] The principle of DNP-NMR had been known for decades, but the technical difficulties associated with constructing an efficient spectrometer were overcome only recently.[220] The possibilities that DNP-NMR has to offer for catalytic studies are yet to be completely explored. There are, nevertheless, several outstanding DNP-NMR studies of heterogeneous catalysts[221−223] and transition metal−zeolite composites, in particular. In this regard, significant attention was attracted by Sn-Beta and other Sn-substituted zeolites.[224,225] The structure of Sn sites in Sn-Beta catalysts under hydration/dehydration conditions is an important factor, governing the reactivity of this promising catalyst. ^{119}Sn NMR is an ideal tool to monitor the structure of Sn sites. Unfortunately, the natural abundance of ^{119}Sn is rather low (8.6%) and extremely long acquisition times are necessary to obtain NMR spectra with acceptable signal-to-noise ratio. Gunther et al. applied indirect DNP-NMR of ^{119}Sn to improve the quality of the signal of 2%Sn-Beta catalysts.[226] The authors identified appropriate combinations of radical and solvent and showed that, at optimized measurement conditions, the acquisition time can be shortened by ca. 2 orders of magnitude, even with the low natural abundance ^{119}Sn in Sn-Beta.

Figure 16 shows that high-quality DNP-enhanced spectra of natural abundant ^{119}Sn can be recorded within a day, while no signal was

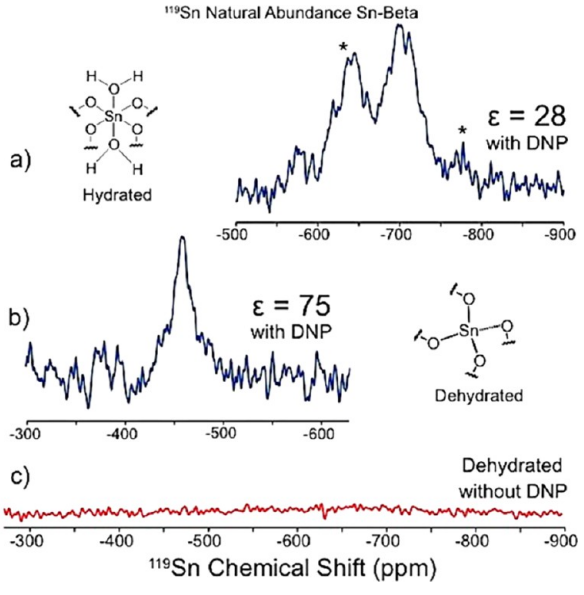

Figure 16. DNP-enhanced ^{119}Sn spectra of hydrated (a) and dehydrated (b) natural abundance Sn-Beta zeolite. Spectra were acquired at 100 K for 18 and 21 h, respectively. ^{119}Sn MAS NMR spectrum of natural abundant dehydrated Sn-Beta zeolite was acquired at 300 K for 246 h. Asterisks denote spinning sidebands. Adapted with permission from ref 226. Copyright 2016 American Chemical Society.

detected with the same sample with regular NMR after more than 10 days of analysis.

Vibrational Spectroscopy. Vibrational methods, including FTIR and Raman spectroscopy, are versatile and robust characterization tools. The most common application of vibrational spectroscopy in analyzing zeolite-based materials is for the FTIR-based determination of the concentration and strength of Brønsted and Lewis acid sites (BAS and LAS). It can be performed either by directly observing the band at ca. 3610 cm^{-1}, related to bridging hydroxyl groups, i.e., BAS, or by using probe molecules such as pyridine (collidine) for quantifying acid sites inside the pores (on the outer surface), CO at liquid nitrogen temperature for elucidating the strength of Brønsted acid sites, etc.[227] FTIR analysis of physi- and chemisorption of probe molecules is also a convenient method for determining the oxidation state and coordination of transition metal sites. Two probe molecules, CO and NO, are particularly useful (especially in combination) and widely applied for the ex situ and operando characterization of metal species. CO can interact with transition metal sites by σ-coordination, when the electron density from the lone pair of CO is transferred to the empty orbitals of a metal atom or by back π-donation from the partially filled d-orbitals. Resulting red or blue shifts from the C−O bond frequency in the gas phase, depending on the strength and nature of corresponding interactions, are useful measures of the properties of the metal phase.[185] In turn, NO, being a radical, is more reactive toward metal sites than CO, and is ultimately a more sensitive probe.[228] The combination of NO and CO for studying catalytic materials is highly advantageous. While CO can be used to probe only certain, i.e., most reactive, metal sites, NO can interact with all metal species of unsaturated coordination. Recently, Sushkevich et al. applied FTIR to study NO and CO adsorption on copper clusters in the pores of a Cu/MOR catalyst for a novel process of two-step anaerobic methane oxidation to methanol.[229] First, by performing CO-FTIR on Cu/MOR samples during different stages of reaction, the authors could find that the Cu(I) sites, formed by reduction of initial Cu(II) sites (which are CO-FTIR invisible) with methane, could be completely restored by the reoxidation with water and that no change occurred to the copper phase during the catalytic cycle, since the frequency of carbonyl and dicarbonyl vibrations remained the same. Further, since NO can be used to detect both Cu(II) and Cu (I), it was possible to track the oxidation state of copper in more detail. In addition, the author found a linear correlation between the number of Brønsted acid sites appearing during reduction of Cu(II) and its detachment from the framework and the number of methoxy species formed upon activation of methane. Eventually, combining the FTIR data with operando XANES measurements and DFT calculations, the entire reaction mechanism was determined as shown by Figure 17.

In relation to transition metal−zeolite composites, Raman spectroscopy is a vibrational spectroscopy technique that is especially powerful for determining the structure and evolution of dispersed metal-oxo complexes, because of high sensitivity to Mo═O and M-O-M vibrations. Importantly, unlike FTIR, Raman spectroscopy is applicable to study processes in aqueous solutions and under high pressure.[230]

Computational Modeling. The conventional preparation methods of zeolite-based transition metal catalysts usually give a variety of different intrazeolite species, which makes it very challenging to unambiguously identify the active sites solely by experiential characterization techniques. Modern computational methodologies provide practical tools to address the structural problem of zeolite catalysis at the molecular level.[231,232] Quantum chemical calculations, including semi-empirical methods, ab initio methods, and density functional theory (DFT), have made significant contributions to elucidate the molecular nature of active sites in zeolite catalysts. DFT calculations are currently considered as the most efficient methods due to a good balance between computational speed and accuracy.

Several important structural problems of extraframework metal species in high-silica zeolites have been successfully resolved by the periodic DFT calculations.[233] Such calculations are carried out within periodic boundary conditions by using real crystal structures of zeolites, in which the structural heterogeneity can be fully addressed at least within a single unit cell approximation. In view of the charge-compensation effect, the distributions of introduced extraframework metal species are largely controlled by the framework Al sitting. Such electrostatic charge-compensation considerations are crucial for metal cations or cationic complexes with a formal charge of +1, which can be readily stabilized via direct charge compensations through the

DOI: 10.1021/acs.chemmater.8b01311
Chem. Mater. 2018, 30, 3177−3198

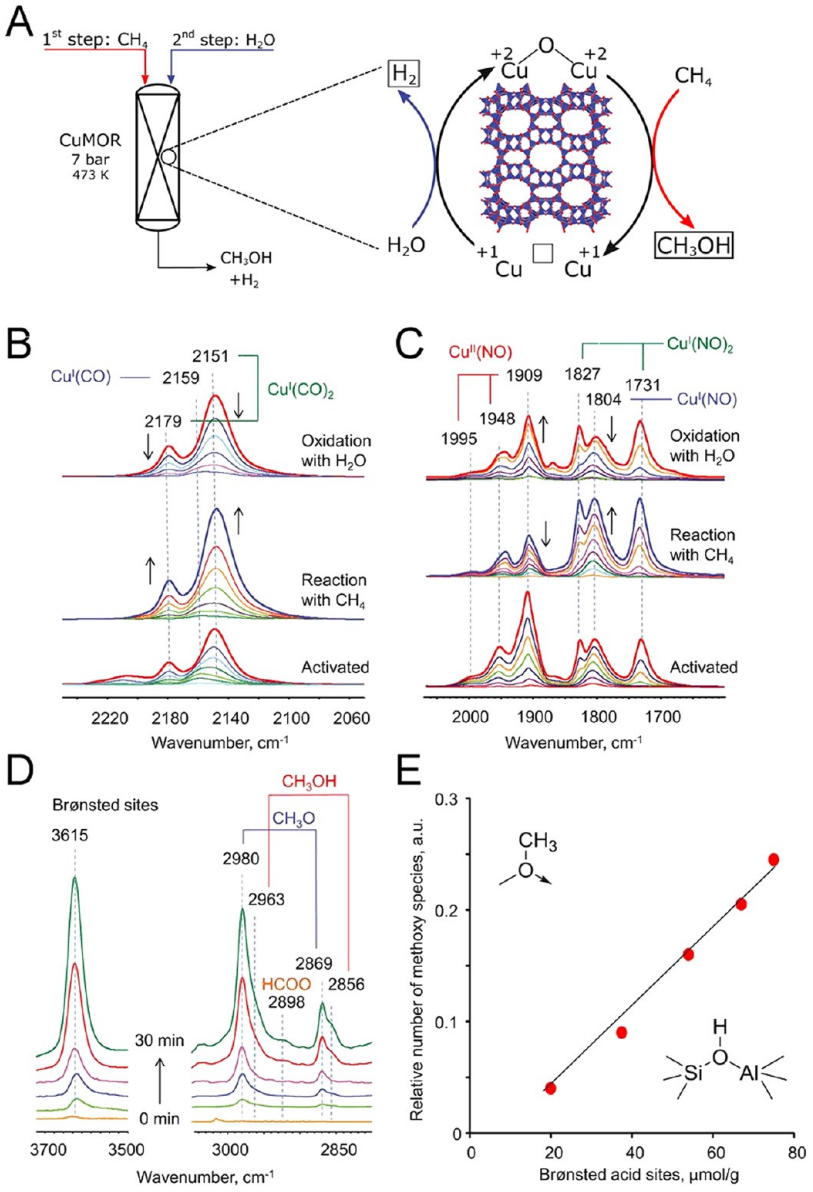

Figure 17. (A) Schematic representation of the reaction conditions of the partial oxidation of methane by water, involving the reduction of the dicopper site of mordenite and providing two electrons to stoichiometrically oxidize methane into methanol. Subsequent reduction of water into hydrogen returns two electrons for the rejuvenation of the mono(μ-oxo)dicopper active core. FTIR spectra of CO (B) and NO (C) adsorbed at 100 K onto CuMOR that was vacuum-activated (bottom), reacted with methane (middle), and reoxidized with water vapor (top). (D) Time-resolved in situ FTIR spectra of surface species formed during the interaction of CuMOR (pretreated in a flow of helium) with 7 bar of methane at 473 K. (E) Relative number of methoxy species versus number of Brønsted acid sites formed during the interaction of methane with CuMOR at 473 K within 5−120 min. Adapted with permission from ref 229. Copyright 2017 AAAS.

coordination with framework anionic $[AlO_2]^-$ sites. However, for metal cations with a charge larger than +1, the direct charge compensation requires the presence of several vicinal lattice Al atoms, which is seldom encountered in practical zeolites and especially in high-silica zeolites. Periodic DFT calculations applied to zeolite systems containing Ga, Zn, Al, Cu, and Fe cations indicated that mononuclear oxygenated and hydroxylated metal complexes are usually less stable than oligonuclear structures.[234] Such mononuclear complexes tend to self-organize into the multinuclear species due to a more favorable coordination environment of the extraframework metal centers in larger clusters. In this case, the direct charge compensation for cationic centers with vicinal lattice $[AlO_2]^-$ becomes less important, and the stability and location of extraframework metal cations are mainly controlled by the favored coordination environment.[235,236] The understanding of extraframework metal species in zeolites can be further progressed by combining DFT calculations with a statistic thermodynamic analysis, in which the effect of temperature, as well as the presence of gaseous reagents such as water and oxygen, can be accounted for.[237,238] Figure 18 illustrates an example of ab initio thermodynamic analysis performed to identify different candidate cationic Cu complexes in ZSM-5 zeolite, which indicates that the formation of Cu complexes with more than two Cu atoms is favored in high-silica ZSM-5 zeolite under oxygen-rich conditions.[239] Such a thermodynamic approach is useful in identifying the nature of intrazeolite species at realistic experimental conditions and even in guiding the design and synthesis of a catalyst with desirable active sites.[36,240] Very recently, the dynamic feature of extraframework metal sites in zeolites under reaction conditions was also highlighted.[241] Combined experimental and computational results indicate that, during the Cu-CHA catalyzed NH_3-SCR reaction, the Cu ions can migrate through zeolite windows with solvated mobility by ammonia, which enables a dynamic generation of multinuclear complexes as

DOI: 10.1021/acs.chemmater.8b01311
Chem. Mater. 2018, 30, 3177−3198

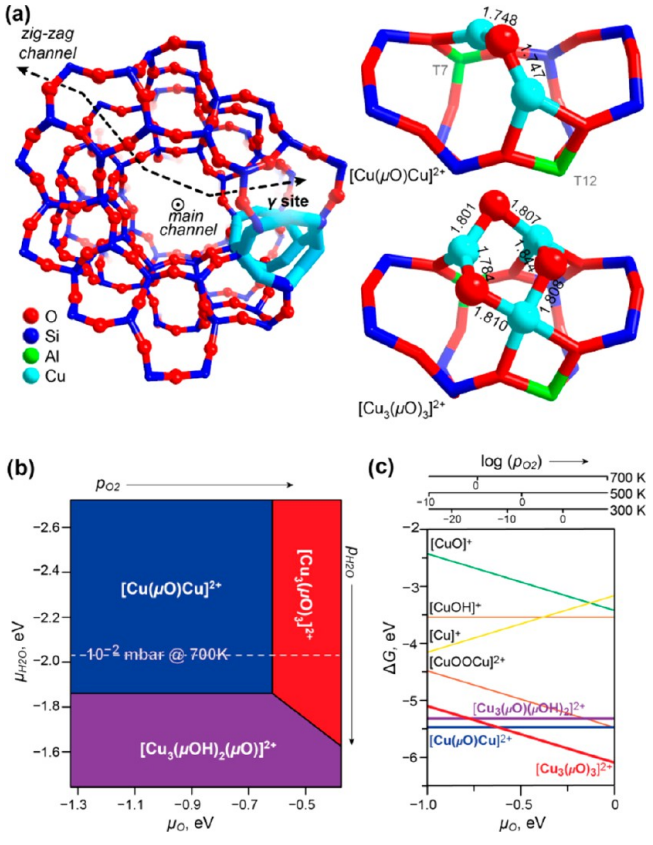

Figure 18. (a) Most stable bi- and trinuclear cationic Cu-oxo clusters in ZSM-5 zeolite as determined by ab initio thermodynamic analysis. Panel (b) shows a 2D projection of the lowest Gibbs free energy $Cu_xO_mH_n$ species in ZSM-5 as a function of oxygen ($\Delta\mu_O$) and water ($\Delta\mu_{H_2O}$) chemical potentials. Panel (c) shows a cross section of the 3D phase diagram at a fixed $\Delta\mu_{H_2O}$, corresponding to 10^{-2} mbar H_2O at 700 K. Adapted with permission from ref 239. Copyright 2016 Elsevier.

active sites for O_2 activation. This represents a distinct phenomenon outside the conventional boundary of single-site heterogeneous catalysts.

The incorporation of a reactive metal center by isomorphous substitution gives rise to Lewis acid lattice sites. The acidity and reactivity of such Lewis sites are affected by the local structure around the reactive lattice heteroatoms, which is determined by the topological and crystallographic T sites in the parent zeolites.[242] Therefore, it is necessary to understand the location, stability, and reactivity of the lattice heteroatoms in zeolite frameworks. Important examples include titanium silicate (TS-1) with MFI topology and Sn-substituted zeolite beta (Sn-BEA). The sitting of Ti in TS-1 material (MFI topology) has been extensively investigated using both experimental and computational approaches.[243,244] However, the reported most populated sites for Ti substitutions usually vary in the literature.[245] A hybrid quantum mechanics (QM)/molecular mechanics (MM) study by Deka et al.[246] proposed that the distribution of Ti in a TS-1 framework may be not determined by the intrinsic stability of the pure TS-1 framework but rather by other thermodynamic or kinetic factors during the synthesis conditions.

Several computational studies have been performed to understand the sitting of heteroatoms in BEA zeolite. A comparative periodic DFT study by Shetty et al.[247] demonstrated that the incorporation of Ti in BEA is more energetically favorable than Sn. Nevertheless, Sn-BEA has a higher Lewis acidity, which makes it a more efficient catalyst for the oxidation reactions than Ti-BEA. Similarly, periodic DFT calculations by Yang et al.[248] showed that the Lewis acidity of Sn- and Zr-substituted BEA is generally quite similar but substantially higher than that of Ti-BEA, and the acidity of particular tetrahedral metal sites strongly depends on the crystallographic location of the heteroatoms. Furthermore, the formation of paired lattice sites was only found in Sn-BEA but not in Ti- or Zr-BEA. Such Sn pairs with enhanced acidity in Sn-BEA were hypothesized to be responsible for its high catalytic activity during sugar conversion.

The framework topology of zeolites affects their catalytic reactivity in view of the varying confinement effect. Recent computational studies emphasized the important role of van der Waals interactions in topologically different zeolites. Li et al.[249] employed periodic DFT calculations to investigate the mechanism of glucose isomerization to fructose catalyzed by framework Sn sites in MOR, BEA, MFI, and MWW zeolites. They found that the framework topology of zeolites has only a minor effect on the intrinsic reactivity of the Sn centers but strongly affects the thermodynamic stabilities of reaction intermediates and products inside the zeolite channels. The increased van der Waals stabilization of such substrates adsorbed in narrow pore zeolites (MFI and MWW) was proposed to limit the intrachannel diffusion, thus resulting in a decrease in the accessibility of the active Sn sites as compared with large-pore zeolites. Similarly, Thang et al.[250] found that the adsorption heats of base probe such as CO on extraframework Li sites increase with the decreasing zeolite channel size because of enlarged dispersion contribution. Moreover, the varying effect on the reactivity of Brønsted acid sites in different zeolite topology was also observed. Periodic DFT calculations by Liu et al.[251] showed that straightforward correlations between Brønsted acidity and reactivity are limited to zeolites with the same topology. For FAU zeolites with varying compositions, the activation energies for the conversion of π-adsorbed isobutene into alkoxy species correlate well with the acid strengths determined by the ammonia adsorption energies. Other zeolites such as MFI and CHA do not follow the scaling relations obtained for FAU, which was proposed to be resulted from different dispersion and steric effects induced by zeolite framework topology.

Computational modeling is a powerful tool to address the structural complexity of zeolite catalysts. The combination of electronic structure calculations with statistic thermodynamic analysis is particularly useful to evaluate the thermodynamic stabilities of metal complexes in zeolites as a function of catalyst activation conditions. However, care has to be taken as the speciation of metal sites in zeolites is often determined by kinetic effects—reactivity, diffusion, solvation, etc. New approaches for studying these effects need to be developed.

CONCLUDING REMARKS

Remarkable recent advances, achieved in synthesis and characterization of well-defined zeolite-based transition metal catalysts, imply a rather bright future for these materials. Further understanding of the metal−zeolite composites will provide a unique opportunity to design ultimately active supported catalysts and bridge the gap between homogeneous and heterogeneous branches of the catalysis science. Rational design of active and selective heterogeneous catalysts has been remaining desirable for generations of chemists. Although it is still somewhat difficult to generalize and rationalize the effects of zeolite topology and metal−zeolite interactions on the catalytic performance, endeavors in this direction are being undertaken.[252] A recent work of Gallego et al. presents an excellent example of such rational design of zeolite catalysts.[253] The authors prepared organic structure-directing agents (SDAs) that resemble in shape and size the transition states of several organic reactions, including isomerization of ethylbenzene to xylenes. Applying the rationally designed template molecules, the authors were able to synthesize several new zeolite topologies, whose catalytic performance in respective reactions was significantly better than that of the benchmark zeolite catalysts. In turn, Rohling et al. recently provided a computational guided optimization of zeolite-based catalysts for Diels−Alder coupling of furanic compounds with

DOI: 10.1021/acs.chemmater.8b01311
Chem. Mater. 2018, 30, 3177−3198

ethylene. The authors established a correlation between catalytic activity of exchanged FAU catalysts and the nature of the used alkali cation. Exchange with K^+ cations was predicted to result in proper interaction with substrate and stabilization of the reaction intermediate and accordingly higher catalytic activity. Experiments, using a series of alkali-exchanged FAU catalysts, fully confirmed this prediction.[254] Unfortunately, such examples of rational design of zeolite-based catalysts are still scarce, and a trial-and-error approach seems to dominate the field. Nevertheless, we are convinced that, together with the current level of synthetic possibilities,[255] further development of computational modeling, advanced spectroscopy tools, and a better general understanding of catalytic processes in a confined space will drive the trial-and-error methods to extinction.

AUTHOR INFORMATION

Corresponding Authors

*E-mail: n.a.kosinov@tue.nl (N.K.).
*E-mail: e.j.m.hensen@tue.nl (E.J.M.H.).
*E-mail: e.a.pidko@tudelft.nl (E.A.P.).

ORCID

Nikolay Kosinov: 0000-0001-8520-4886
Chong Liu: 0000-0003-0311-8744
Emiel J. M. Hensen: 0000-0002-9754-2417
Evgeny A. Pidko: 0000-0001-9242-9901

Present Address

[‖]Schuit Institute of Catalysis, Laboratory of Inorganic Materials Chemistry, Eindhoven University of Technology, P.O. Box 513, 5600 MB Eindhoven, The Netherlands.

Notes

The authors declare no competing financial interest.

ACKNOWLEDGMENTS

This project has received funding from the European Research Council (ERC) under the European Union's Horizon 2020 research and innovation programme (grant agreement No. 725686). The authors would like to thank Alexey Kubarev (KU Leuven), Arno van Hoof (TU Eindhoven), and Wilbert Vrijburg (TU Eindhoven) for valuable discussion.

REFERENCES

(1) Böhme, D. K.; Schwarz, H. Gas-Phase Catalysis by Atomic and Cluster Metal Ions: The Ultimate Single-Site Catalysts. *Angew. Chem., Int. Ed.* **2005**, *44*, 2336−2354.
(2) Yang, X. F.; Wang, A.; Qiao, B.; Li, J.; Liu, J.; Zhang, T. Single-Atom Catalysts: A New Frontier in Heterogeneous Catalysis. *Acc. Chem. Res.* **2013**, *46*, 1740−1748.
(3) Qin, R.; Liu, P.; Fu, G.; Zheng, N. Strategies for Stabilizing Atomically Dispersed Metal Catalysts. *Small Methods* **2018**, *2*, 1700286.
(4) Corma, A. Attempts to Fill the Gap Between Enzymatic, Homogeneous, and Heterogeneous Catalysis. *Catal. Rev.: Sci. Eng.* **2004**, *46*, 369−417.
(5) Smit, B.; Maesen, T. L. M. Towards a Molecular Understanding of Shape Selectivity. *Nature* **2008**, *451*, 671−678.
(6) Csicsery, S M. Shape-Selective Catalysis in Zeolites. *Zeolites* **1984**, *4*, 202−213.
(7) Cruciani, G. Zeolites upon Heating: Factors Governing Their Thermal Stability and Structural Changes. *J. Phys. Chem. Solids* **2006**, *67*, 1973−1994.
(8) Blakeman, P. G.; Burkholder, E. M.; Chen, H. Y.; Collier, J. E.; Fedeyko, J. M.; Jobson, H.; Rajaram, R. R. The Role of Pore Size on the Thermal Stability of Zeolite Supported Cu SCR Catalysts. *Catal. Today* **2014**, *231*, 56−63.
(9) Kosinov, N.; Auffret, C.; Gücüyener, C.; Szyja, B. M.; Gascon, J.; Kapteijn, F.; Hensen, E. J. M. High Flux High-Silica SSZ-13 Membrane for CO_2 Separation. *J. Mater. Chem. A* **2014**, *2*, 13083−13092.
(10) Prodinger, S.; Shi, H.; Eckstein, S.; Hu, J. Z.; Olarte, M. V.; Camaioni, D. M.; Derewinski, M. A.; Lercher, J. A. Stability of Zeolites in Aqueous Phase Reactions. *Chem. Mater.* **2017**, *29*, 7255−7262.
(11) Vogt, E. T. C.; Weckhuysen, B. M. Fluid Catalytic Cracking: Recent Developments on the Grand Old Lady of Zeolite Catalysis. *Chem. Soc. Rev.* **2015**, *44*, 7342−7370.
(12) Blay, V.; Louis, B.; Miravalles, R.; Yokoi, T.; Peccatiello, K. A.; Clough, M.; Yilmaz, B. Engineering Zeolites for Catalytic Cracking to Light Olefins. *ACS Catal.* **2017**, *7*, 6542−6566.
(13) Ennaert, T.; van Aelst, J.; Dijkmans, J.; De Clercq, R.; Schutyser, W.; Dusselier, M.; Verboekend, D.; Sels, B. F. Potential and Challenges of Zeolite Chemistry in the Catalytic Conversion of Biomass. *Chem. Soc. Rev.* **2016**, *45*, 584−611.
(14) Su, F.; Guo, Y. Advancements in Solid Acid Catalysts for Biodiesel Production. *Green Chem.* **2014**, *16*, 2934−2957.
(15) Olivos Suarez, A. I.; Szécsényi, Á.; Hensen, E. J. M.; Ruiz-Martínez, J.; Pidko, E. A.; Gascon, J. Strategies for the Direct Catalytic Valorization of Methane Using Heterogeneous Catalysis: Challenges and Opportunities. *ACS Catal.* **2016**, *6*, 2965−2981.
(16) Schwach, P.; Pan, X.; Bao, X. Direct Conversion of Methane to Value-Added Chemicals over Heterogeneous Catalysts: Challenges and Prospects. *Chem. Rev.* **2017**, *117*, 8497−8520.
(17) van Speybroeck, V.; De Wispelaere, K.; van der Mynsbrugge, J.; Vandichel, M.; Hemelsoet, K.; Waroquier, M. First Principle Chemical Kinetics in Zeolites: The Methanol-to-Olefin Process as a Case Study. *Chem. Soc. Rev.* **2014**, *43*, 7326−7357.
(18) Olsbye, U.; Svelle, S.; Bjørgen, M.; Beato, P.; Janssens, T. V. W.; Joensen, F.; Bordiga, S.; Lillerud, K. P. Conversion of Methanol to Hydrocarbons: How Zeolite Cavity and Pore Size Controls Product Selectivity. *Angew. Chem., Int. Ed.* **2012**, *51*, 5810−5831.
(19) Ilias, S.; Bhan, A. Mechanism of the Catalytic Conversion of Methanol to Hydrocarbons. *ACS Catal.* **2013**, *3*, 18−31.
(20) Beale, A. M.; Gao, F.; Lezcano-Gonzalez, I.; Peden, C. H. F.; Szanyi, J. Recent Advances in Automotive Catalysis for NO_x Emission Control by Small-Pore Microporous Materials. *Chem. Soc. Rev.* **2015**, *44*, 7371−7405.
(21) Zhang, R.; Liu, N.; Lei, Z.; Chen, B. Selective Transformation of Various Nitrogen-Containing Exhaust Gases toward N_2 over Zeolite Catalysts. *Chem. Rev.* **2016**, *116*, 3658−3721.
(22) Granger, P.; Parvulescu, V. I. Catalytic NO_x Abatement Systems for Mobile Sources: From Three-Way to Lean Burn after-Treatment Technologies. *Chem. Rev.* **2011**, *111*, 3155−3207.
(23) http://www.iza-structure.org/databases.
(24) Gao, J.; Zheng, Y.; Jehng, J.-M.; Tang, Y.; Wachs, I. E.; Podkolzin, S. G. Identification of Molybdenum Oxide Nanostructures on Zeolites for Natural Gas Conversion. *Science* **2015**, *348*, 686−690.
(25) Zheng, H.; Ma, D.; Bao, X.; Hu, Z. H.; Kwak, J. H.; Wang, Y.; Peden, C. H. F. Direct Observation of the Active Center for Methane Dehydroaromatization Using an Ultrahigh Field ^{95}Mo NMR Spectroscopy. *J. Am. Chem. Soc.* **2008**, *130*, 3722−3723.
(26) Kosinov, N.; Coumans, F. J. A. G.; Uslamin, E. A.; Wijpkema, A. S. G.; Mezari, B.; Hensen, E. J. M. Methane Dehydroaromatization by Mo/HZSM-5: Mono- or Bifunctional Catalysis? *ACS Catal.* **2017**, *7*, 520−529.
(27) Zhang, J.; Wang, L.; Shao, Y.; Wang, Y.; Gates, B. C.; Xiao, F. S. A Pd at Zeolite Catalyst for Nitroarene Hydrogenation with High Product Selectivity by Sterically Controlled Adsorption in the Zeolite Micropores. *Angew. Chem., Int. Ed.* **2017**, *56*, 9747−9751.
(28) Zhan, B. Z.; Iglesia, E. RuO_2 Clusters within LTA Zeolite Cages: Consequences of Encapsulation on Catalytic Reactivity and Selectivity. *Angew. Chem., Int. Ed.* **2007**, *46*, 3697−3700.
(29) Clark, L. A.; Sierka, M.; Sauer, J. Computational Elucidation of the Transition State Shape Selectivity Phenomenon. *J. Am. Chem. Soc.* **2004**, *126*, 936−947.

DOI: 10.1021/acs.chemmater.8b01311
Chem. Mater. 2018, 30, 3177−3198

(30) Collett, C. H.; Mcgregor, J. Things Go Better with Coke: The Beneficial Role of Carbonaceous Deposits in Heterogeneous Catalysis. *Catal. Sci. Technol.* **2016**, *6*, 363−378.
(31) White, J. L. Methanol-to-Hydrocarbon Chemistry: The Carbon Pool (R)evolution. *Catal. Sci. Technol.* **2011**, *1*, 1630−1635.
(32) Kosinov, N.; Wijpkema, A. S. G.; Uslamin, E.; Rohling, R.; Coumans, F. J. A. G.; Mezari, B.; Parastaev, A.; Poryvaev, A. S.; Fedin, M. V.; Pidko, E. A.; Hensen, E. J. M. Confined Carbon Mediating Dehydroaromatization of Methane over Mo/ZSM-5. *Angew. Chem., Int. Ed.* **2018**, *57*, 1016−1020.
(33) Yilmaz, B.; Müller, U. Catalytic Applications of Zeolites in Chemical Industry. *Top. Catal.* **2009**, *52*, 888−895.
(34) Tomkins, P.; Mansouri, A.; Bozbag, S. E.; Krumeich, F.; Park, M. B.; Alayon, E. M. C.; Ranocchiari, M.; van Bokhoven, J. A. Isothermal Cyclic Conversion of Methane into Methanol over Copper-Exchanged Zeolite at Low Temperature. *Angew. Chem., Int. Ed.* **2016**, *55*, 5467−5471.
(35) Elwell, C. E.; Gagnon, N. L.; Neisen, B. D.; Dhar, D.; Spaeth, A. D.; Yee, G. M.; Tolman, W. B. Copper-Oxygen Complexes Revisited: Structures, Spectroscopy, and Reactivity. *Chem. Rev.* **2017**, *117*, 2059−2107.
(36) Grundner, S.; Markovits, M. A. C.; Li, G.; Tromp, M.; Pidko, E. A.; Hensen, E. J. M.; Jentys, A.; Sanchez-Sanchez, M.; Lercher, J. A. Single-Site Trinuclear Copper Oxygen Clusters in Mordenite for Selective Conversion of Methane to Methanol. *Nat. Commun.* **2015**, *6*, 7546.
(37) Ozin, G. A.; Ozkar, S. Zeolates: A Coordination Chemistry View of Metal-Ligand Bonding in Zeolite Guest-Host Inclusion Compounds. *Chem. Mater.* **1992**, *4*, 511−521.
(38) Schoonheydt, R. A.; Geerlings, P.; Pidko, E. A.; van Santen, R. A. The Framework Basicity of Zeolites. *J. Mater. Chem.* **2012**, *22*, 18705−18717.
(39) Li, S.; Tuel, A.; Meunier, F.; Aouine, M.; Farrusseng, D. Platinum Nanoparticles Entrapped in Zeolite Nanoshells as Active and Sintering-Resistant Arene Hydrogenation Catalysts. *J. Catal.* **2015**, *332*, 25−30.
(40) Primo, A.; Garcia, H. Zeolites as Catalysts in Oil Refining. *Chem. Soc. Rev.* **2014**, *43*, 7548−7561.
(41) Perego, C.; Calemma, V.; Pollesel, P. Naphtha Reforming and Upgrading of Diesel Fractions. In *Zeolites and Catalysis*; Wiley-VCH Verlag GmbH & Co. KGaA: Weinheim, Germany, 2010; Vol. 2, pp 585−621.
(42) Caeiro, G.; Carvalho, R. H.; Wang, X.; Lemos, M. A. N. D. A.; Lemos, F.; Guisnet, M.; Ramôa Ribeiro, F. Activation of C_2-C_4 Alkanes over Acid and Bifunctional Zeolite Catalysts. *J. Mol. Catal. A: Chem.* **2006**, *255*, 131−158.
(43) Ismagilov, Z. R.; Matus, E. V.; Tsikoza, L. T. Direct Conversion of Methane on Mo/ZSM-5 Catalysts to Produce Benzene and Hydrogen: Achievements and Perspectives. *Energy Environ. Sci.* **2008**, *1*, 526−541.
(44) Han, B.; Yang, Y.; Xu, Y.; Etim, U. J.; Qiao, K.; Xu, B.; Yan, Z. A Review of the Direct Oxidation of Methane to Methanol. *Chin. J. Catal.* **2016**, *37*, 1206−1215.
(45) Taarning, E.; Osmundsen, C. M.; Yang, X.; Voss, B.; Andersen, S. I.; Christensen, C. H. Zeolite-Catalyzed Biomass Conversion to Fuels and Chemicals. *Energy Environ. Sci.* **2011**, *4*, 793−804.
(46) Brandenberger, S.; Kröcher, O.; Tissler, A.; Althoff, R. The State of the Art in Selective Catalytic Reduction of NO_x by Ammonia Using Metal-Exchanged Zeolite Catalysts. *Catal. Rev.: Sci. Eng.* **2008**, *50*, 492−531.
(47) Zhang, L.; Peng, Y.; Zhang, J.; Chen, L.; Meng, X.; Xiao, F. S. Adsorptive and Catalytic Properties in the Removal of Volatile Organic Compounds over Zeolite-Based Materials. *Chin. J. Catal.* **2016**, *37*, 800−809.
(48) Shahidi, D.; Roy, R.; Azzouz, A. Advances in Catalytic Oxidation of Organic Pollutants - Prospects for Thorough Mineralization by Natural Clay Catalysts. *Appl. Catal., B* **2015**, *174*−*175*, 277−292.
(49) Centi, G.; Perathoner, S. Environmental Catalysis over Zeolites. *Zeolites Catal. Synth. React. Appl.* **2010**, *2*, 745−774.
(50) Sartipi, S.; Makkee, M.; Kapteijn, F.; Gascon, J. Catalysis Engineering of Bifunctional Solids for the One-Step Synthesis of Liquid Fuels from Syngas: A Review. *Catal. Sci. Technol.* **2014**, *4*, 893−907.
(51) Perego, C.; Carati, A.; Ingallina, P.; Mantegazza, M. A.; Bellussi, G. Production of Titanium Containing Molecular Sieves and Their Application in Catalysis. *Appl. Catal., A* **2001**, *221*, 63−72.
(52) Fukuzumi, S.; Ohkubo, K. One-Step Selective Hydroxylation of Benzene to Phenol. *Asian J. Org. Chem.* **2015**, *4*, 836−845.
(53) Cui, T. L.; Ke, W. Y.; Zhang, W. B.; Wang, H. H.; Li, X. H.; Chen, J. S. Encapsulating Palladium Nanoparticles Inside Mesoporous MFI Zeolite Nanocrystals for Shape-Selective Catalysis. *Angew. Chem., Int. Ed.* **2016**, *55*, 9178−9182.
(54) van De Vyver, S.; Román-Leshkov, Y. Metalloenzyme-Like Zeolites as Lewis Acid Catalysts for C-C Bond Formation. *Angew. Chem., Int. Ed.* **2015**, *54*, 12554−12561.
(55) Moliner, M. State of the Art of Lewis Acid-Containing Zeolites: Lessons from Fine Chemistry to New Biomass Transformation Processes. *Dalt. Trans.* **2014**, *43*, 4197−4208.
(56) Gao, F.; Walter, E. D.; Washton, N. M.; Szanyi, J.; Peden, C. H. F. Synthesis and Evaluation of Cu/SAPO-34 Catalysts for NH_3-SCR 2: Solid-State Ion Exchange and One-Pot Synthesis. *Appl. Catal., B* **2015**, *162*, 501−514.
(57) Iwasaki, M.; Yamazaki, K.; Banno, K.; Shinjoh, H. Characterization of Fe/ZSM-5 deNO_x Catalysts Prepared by Different Methods: Relationships between Active Fe Sites and NH_3-SCR Performance. *J. Catal.* **2008**, *260*, 205−216.
(58) Fricke, R.; Kosslick, H.; Lischke, G.; Richter, M. Incorporation of Gallium into Zeolites: Syntheses, Properties and Catalytic Application. *Chem. Rev.* **2000**, *100*, 2303−2405.
(59) Wang, D.; Gao, F.; Peden, C. H. F.; Li, J.; Kamasamudram, K.; Epling, W. S. Selective Catalytic Reduction of NOx with NH_3 over a Cu-SSZ-13 Catalyst Prepared by a Solid-State Ion-Exchange Method. *ChemCatChem* **2014**, *6*, 1579−1583.
(60) Shwan, S.; Skoglundh, M.; Lundegaard, L. F.; Tiruvalam, R. R.; Janssens, T. V. W.; Carlsson, A.; Vennestrøm, P. N. R. Solid-State Ion-Exchange of Copper into Zeolites Facilitated by Ammonia at Low Temperature. *ACS Catal.* **2015**, *5*, 16−19.
(61) Serp, P.; Kalck, P.; Feurer, R. Chemical Vapor Deposition Methods for the Controlled Preparation of Supported Catalytic Materials. *Chem. Rev.* **2002**, *102*, 3085−3128.
(62) Almutairi, S. M. T.; Mezari, B.; Magusin, P. C. M. M.; Pidko, E. A.; Hensen, E. J. M. Structure and Reactivity of Zn-Modified ZSM-5 Zeolites: The Importance of Clustered Cationic Zn Complexes. *ACS Catal.* **2012**, *2*, 71−83.
(63) Li, P.; Liu, G.; Wu, H.; Liu, Y.; Jiang, J. G.; Wu, P. Postsynthesis and Selective Oxidation Properties of Nanosized Sn-Beta Zeolite. *J. Phys. Chem. C* **2011**, *115*, 3663−3670.
(64) Rane, N.; Kersbulck, M.; van Santen, R. A.; Hensen, E. J. M. Cracking of n-Heptane over Brønsted Acid Sites and Lewis Acid Ga Sites in ZSM-5 Zeolite. *Microporous Mesoporous Mater.* **2008**, *110*, 279−291.
(65) Kusakari, T.; Sasaki, T.; Iwasawa, Y. Selective Oxidation of Benzene to Phenol with Molecular Oxygen on Rhenium/zeolite Catalysts. *Chem. Commun.* **2004**, *6*, 992−993.
(66) Zhang, J.; Tu, R.; Goto, T. Precipitation of Ni Nanoparticle on Al_2O_3 Powders by Novel Rotary Chemical Vapor Deposition. *J. Ceram. Soc. Jpn.* **2013**, *121*, 226−229.
(67) Gates, B. Supported Metal Cluster Catalysts. *J. Mol. Catal. A: Chem.* **2000**, *163*, 55−65.
(68) Serna, P.; Yardimci, D.; Kistler, J. D.; Gates, B. C. Formation of Supported Rhodium Clusters from Mononuclear Rhodium Complexes Controlled by the Support and Ligands on Rhodium. *Phys. Chem. Chem. Phys.* **2014**, *16*, 1262−1270.
(69) Lu, J.; Aydin, C.; Browning, N. D.; Wang, L.; Gates, B. C. Sinter-Resistant Catalysts: Supported Iridium Nanoclusters with Intrinsically Limited Sizes. *Catal. Lett.* **2012**, *142*, 1445−1451.
(70) Hao, Y.; Gates, B. C. Activation of Dimethyl Gold Complexes on MgO for CO Oxidation: Removal of Methyl Ligands and

DOI: 10.1021/acs.chemmater.8b01311
Chem. Mater. 2018, 30, 3177−3198

Formation of Catalytically Active Gold Clusters. *J. Catal.* **2009**, *263*, 83−91.
(71) Kistler, J. D.; Chotigkrai, N.; Xu, P.; Enderle, B.; Praserthdam, P.; Chen, C. Y.; Browning, N. D.; Gates, B. C. A Single-Site Platinum CO Oxidation Catalyst in Zeolite KLTL: Microscopic and Spectroscopic Determination of the Locations of the Platinum Atoms. *Angew. Chem., Int. Ed.* **2014**, *53*, 8904−8907.
(72) Martinez-Macias, C.; Xu, P.; Hwang, S. J.; Lu, J.; Chen, C. Y.; Browning, N. D.; Gates, B. C. Iridium Complexes and Clusters in Dealuminated Zeolite HY: Distribution between Crystalline and Impurity Amorphous Regions. *ACS Catal.* **2014**, *4*, 2662−2666.
(73) Meng, L.; Zhu, X.; Mezari, B.; Pestman, R.; Wannapakdee, W.; Hensen, E. J. M. On the Role of Acidity in Bulk and Nanosheet [T]MFI (T=Al^{3+}, Ga^{3+}, Fe^{3+}, B^{3+}) Zeolites in the Methanol-to-Hydrocarbons Reaction. *ChemCatChem* **2017**, *9*, 3942−3954.
(74) Wu, Y.; Wang, J.; Liu, P.; Zhang, W.; Gu, J.; Wang, X. Framework-Substituted Lanthanide MCM-22 Zeolite: Synthesis and Characterization. *J. Am. Chem. Soc.* **2010**, *132*, 17989−17991.
(75) Lee, W. S.; Cem Akatay, M.; Stach, E. A.; Ribeiro, F. H.; Nicholas Delgass, W. Gas-Phase Epoxidation of Propylene in the Presence of H_2 and O_2 over Small Gold Ensembles in Uncalcined TS-1. *J. Catal.* **2014**, *313*, 104−112.
(76) Corma, A.; Camblor, M. A.; Esteve, P.; Martínez, A.; Pérez-Pariente, J. Activity of Ti-Beta Catalyst for the Selective Oxidation of Alkenes and Alkanes. *J. Catal.* **1994**, *145*, 151−158.
(77) Blasco, T.; Camblor, M. A.; Corma, A.; Esteve, P.; Guil, J. M.; Martínez, A.; Perdigón-Melón, J. A.; Valencia, S. Direct Synthesis and Characterization of Hydrophobic Aluminum-Free Ti−Beta Zeolite. *J. Phys. Chem. B* **1998**, *102*, 75−88.
(78) van der Graaff, W. N. P.; Tempelman, C. H. L.; Li, G.; Mezari, B.; Kosinov, N.; Pidko, E. A.; Hensen, E. J. M. Competitive Adsorption of Substrate and Solvent in Sn-Beta Zeolite During Sugar Isomerization. *ChemSusChem* **2016**, *9*, 3145−3149.
(79) Huber, G. W.; Corma, A. Synergies between Bio- and Oil Refineries for the Production of Fuels from Biomass. *Angew. Chem., Int. Ed.* **2007**, *46*, 7184−7201.
(80) Román-Leshkov, Y.; Davis, M. E. Activation of Carbonyl-Containing Molecules with Solid Lewis Acids in Aqueous Media. *ACS Catal.* **2011**, *1*, 1566−1580.
(81) Kosinov, N.; Sripathi, V. G. P.; Hensen, E. J. M. Improving Separation Performance of High-Silica Zeolite Membranes by Surface Modification with Triethoxyfluorosilane. *Microporous Mesoporous Mater.* **2014**, *194*, 24−30.
(82) Corma, A.; Nemeth, L. T.; Renz, M.; Valencia, S. Sn-Zeolite Beta as a Heterogeneous Chemoselective Catalyst for Baeyer-Villiger Oxidations. *Nature* **2001**, *412*, 423−425.
(83) Hammond, C.; Conrad, S.; Hermans, I. Simple and Scalable Preparation of Highly Active Lewis Acidic Sn-*β*. *Angew. Chem., Int. Ed.* **2012**, *51*, 11736−11739.
(84) van Der Graaff, W. N. P.; Li, G.; Mezari, B.; Pidko, E. A.; Hensen, E. J. M. Synthesis of Sn-Beta with Exclusive and High Framework Sn Content. *ChemCatChem* **2015**, *7*, 1152−1160.
(85) Meng, X.; Xiao, F. S. Green Routes for Synthesis of Zeolites. *Chem. Rev.* **2014**, *114*, 1521−1543.
(86) Cundy, C. S.; Cox, P. A. The Hydrothermal Synthesis of Zeolites: History and Development from the Earliest Days to the Present Time. *Chem. Rev.* **2003**, *103*, 663−702.
(87) Farrusseng, D.; Tuel, A. Zeolite-Encapsulated Catalysts. In *Encapsulated Catalysts*; Elsevier: London, 2017; pp 335−386.
(88) Wu, Z.; Goel, S.; Choi, M.; Iglesia, E. Hydrothermal Synthesis of LTA-Encapsulated Metal Clusters and Consequences for Catalyst Stability, Reactivity, and Selectivity. *J. Catal.* **2014**, *311*, 458−468.
(89) Otto, T.; Zones, S. I.; Hong, Y.; Iglesia, E. Synthesis of Highly Dispersed Cobalt Oxide Clusters Encapsulated within LTA Zeolites. *J. Catal.* **2017**, *356*, 173−185.
(90) Otto, T.; Zones, S. I.; Iglesia, E. Challenges and Strategies in the Encapsulation and Stabilization of Monodisperse Au Clusters within Zeolites. *J. Catal.* **2016**, *339*, 195−208.
(91) Wang, N.; Sun, Q.; Bai, R.; Li, X.; Guo, G.; Yu, J. In Situ Confinement of Ultrasmall Pd Clusters within Nanosized Silicalite-1 Zeolite for Highly Efficient Catalysis of Hydrogen Generation. *J. Am. Chem. Soc.* **2016**, *138*, 7484−7487.
(92) Goel, S.; Wu, Z.; Zones, S. I.; Iglesia, E. Synthesis and Catalytic Properties of Metal Clusters Encapsulated within Small-Pore (SOD, GIS, ANA) Zeolites. *J. Am. Chem. Soc.* **2012**, *134*, 17688−17695.
(93) Sun, Q.; Wang, N.; Bing, Q.; Si, R.; Liu, J.; Bai, R.; Zhang, P.; Jia, M.; Yu, J. Subnanometric Hybrid Pd-$M(OH)_2$, M = Ni, Co, Clusters in Zeolites as Highly Efficient Nanocatalysts for Hydrogen Generation. *Chem.* **2017**, *3*, 477−493.
(94) Otto, T.; Ramallo-López, J. M.; Giovanetti, L. J.; Requejo, F. G.; Zones, S. I.; Iglesia, E. Synthesis of Stable Monodisperse AuPd, AuPt, and PdPt Bimetallic Clusters Encapsulated within LTA-Zeolites. *J. Catal.* **2016**, *342*, 125−137.
(95) Moliner, M.; Gabay, J. E.; Kliewer, C. E.; Carr, R. T.; Guzman, J.; Casty, G. L.; Serna, P.; Corma, A. Reversible Transformation of Pt Nanoparticles into Single Atoms inside High-Silica Chabazite Zeolite. *J. Am. Chem. Soc.* **2016**, *138*, 15743−15750.
(96) Gao, D.; Zheng, A.; Zhang, X.; Sun, H.; Dai, X.; Yang, Y.; Wang, H.; Qin, Y.; Xu, S.; Duan, A. Mercaptosilane-Assisted Synthesis of Sub-Nanosized Pt Particles within Hierarchically Porous ZSM-5/SBA-15 Materials and Their Enhanced Hydrogenation Properties. *Nanoscale* **2015**, *7*, 10918−10924.
(97) Laursen, A. B.; Højholt, K. T.; Lundegaard, L. F.; Simonsen, S. B.; Helveg, S.; Schüth, F.; Paul, M.; Grunwaldt, J. D.; Kegnæs, S.; Christensen, C. H.; Egeblad, K. Substrate Size-Selective Catalysis with Zeolite-Encapsulated Gold Nanoparticles. *Angew. Chem., Int. Ed.* **2010**, *49*, 3504−3507.
(98) Gu, J.; Zhang, Z.; Hu, P.; Ding, L.; Xue, N.; Peng, L.; Guo, X.; Lin, M.; Ding, W. Platinum Nanoparticles Encapsulated in MFI Zeolite Crystals by a Two-Step Dry Gel Conversion Method as a Highly Selective Hydrogenation Catalyst. *ACS Catal.* **2015**, *5*, 6893−6901.
(99) Goel, S.; Zones, S. I.; Iglesia, E. Encapsulation of Metal Clusters within MFI via Interzeolite Transformations and Direct Hydrothermal Syntheses and Catalytic Consequences of Their Confinement. *J. Am. Chem. Soc.* **2014**, *136*, 15280−15290.
(100) Corma, A.; Fornes, V.; Pergher, S. B.; Maesen, T. L. M.; Buglass, J. G. Delaminated Zeolite Precursors as Selective Acidic Catalysts. *Nature* **1998**, *396*, 353−356.
(101) Liu, L.; Díaz, U.; Arenal, R.; Agostini, G.; Concepción, P.; Corma, A. Generation of Subnanometric Platinum with High Stability during Transformation of a 2D Zeolite into 3D. *Nat. Mater.* **2017**, *16*, 132−138.
(102) Pagis, C.; Morgado Prates, A. R.; Farrusseng, D.; Bats, N.; Tuel, A. Hollow Zeolite Structures: An Overview of Synthesis Methods. *Chem. Mater.* **2016**, *28*, 5205−5223.
(103) Fodor, D.; Ishikawa, T.; Krumeich, F.; van Bokhoven, J. A. Synthesis of Single Crystal Nanoreactor Materials with Multiple Catalytic Functions by Incipient Wetness Impregnation and Ion Exchange. *Adv. Mater.* **2015**, *27*, 1919−1923.
(104) Li, S.; Tuel, A.; Laprune, D.; Meunier, F.; Farrusseng, D. Transition-Metal Nanoparticles in Hollow Zeolite Single Crystals as Bifunctional and Size-Selective Hydrogenation Catalysts. *Chem. Mater.* **2015**, *27*, 276−282.
(105) Li, S.; Burel, L.; Aquino, C.; Tuel, A.; Morfin, F.; Rousset, J.-L.; Farrusseng, D. Ultimate Size Control of Encapsulated Gold Nanoparticles. *Chem. Commun.* **2013**, *49*, 8507−8509.
(106) Li, S.; Boucheron, T.; Tuel, A.; Farrusseng, D.; Meunier, F. Size-Selective Hydrogenation at the Subnanometer Scale over Platinum Nanoparticles Encapsulated in Silicalite-1 Single Crystal Hollow Shells. *Chem. Commun.* **2014**, *50*, 1824−1826.
(107) Roiban, L.; Li, S.; Aouine, M.; Tuel, A.; Farrusseng, D.; Epicier, T. Fast " Operando " Electron Nanotomography. *J. Microsc.* **2018**, *269*, 117−126.
(108) Iida, T.; Shetty, M.; Murugappan, K.; Wang, Z.; Ohara, K.; Wakihara, T.; Román-Leshkov, Y. Encapsulation of Molybdenum Carbide Nanoclusters inside Zeolite Micropores Enables Synergistic

DOI: 10.1021/acs.chemmater.8b01311
Chem. Mater. 2018, 30, 3177−3198

Bifunctional Catalysis for Anisole Hydrodeoxygenation. *ACS Catal.* **2017**, *7*, 8147−8151.
(109) Zhang, W. H.; Shi, J. L.; Chen, H. R.; Hua, Z. L.; Yan, D. S. Synthesis and Characterization of Nanosized ZnS Confined in Ordered Mesoporous Silica. *Chem. Mater.* **2001**, *13*, 648−654.
(110) Dědeček, J.; Sobalík, Z.; Wichterlová, B. Siting and Distribution of Framework Aluminium Atoms in Silicon-Rich Zeolites and Impact on Catalysis. *Catal. Rev.: Sci. Eng.* **2012**, *54*, 135−223.
(111) Yokoi, T.; Mochizuki, H.; Namba, S.; Kondo, J. N.; Tatsumi, T. Control of the Al Distribution in the Framework of ZSM-5 Zeolite and Its Evaluation by Solid-State NMR Technique and Catalytic Properties. *J. Phys. Chem. C* **2015**, *119*, 15303−15315.
(112) Yokoi, T.; Mochizuki, H.; Biligetu, T.; Wang, Y.; Tatsumi, T. Unique Al Distribution in the MFI Framework and Its Impact on Catalytic Properties. *Chem. Lett.* **2017**, *46*, 798−800.
(113) Biligetu, T.; Wang, Y.; Nishitoba, T.; Otomo, R.; Park, S.; Mochizuki, H.; Kondo, J. N.; Tatsumi, T.; Yokoi, T. Al Distribution and Catalytic Performance of ZSM-5 Zeolites Synthesized with Various Alcohols. *J. Catal.* **2017**, *353*, 1−10.
(114) Pinar, A. B.; Gómez-Hortigüela, L.; McCusker, L. B.; Pérez-Pariente, J. Controlling the Aluminum Distribution in the Zeolite Ferrierite via the Organic Structure Directing Agent. *Chem. Mater.* **2013**, *25*, 3654−3661.
(115) Di Iorio, J. R.; Gounder, R. Controlling the Isolation and Pairing of Aluminum in Chabazite Zeolites Using Mixtures of Organic and Inorganic Structure-Directing Agents. *Chem. Mater.* **2016**, *28*, 2236−2247.
(116) Liu, M.; Yokoi, T.; Yoshioka, M.; Imai, H.; Kondo, J. N.; Tatsumi, T. Differences in Al Distribution and Acidic Properties between RTH-Type Zeolites Synthesized with OSDAs and without OSDAs. *Phys. Chem. Chem. Phys.* **2014**, *16*, 4155−4164.
(117) Fletcher, R. E.; Ling, S.; Slater, B. Violations of Löwenstein's Rule in Zeolites. *Chem. Sci.* **2017**, *8*, 7483−7491.
(118) Di Iorio, J. R.; Nimlos, C. T.; Gounder, R. Introducing Catalytic Diversity into Single-Site Chabazite Zeolites of Fixed Composition via Synthetic Control of Active Site Proximity. *ACS Catal.* **2017**, *7*, 6663−6674.
(119) Dedecek, J.; Balgová, V.; Pashkova, V.; Klein, P.; Wichterlová, B. Synthesis of ZSM-5 Zeolites with Defined Distribution of Al Atoms in the Framework and Multinuclear MAS NMR Analysis of the Control of Al Distribution. *Chem. Mater.* **2012**, *24*, 3231−3239.
(120) Pashkova, V.; Klein, P.; Dedecek, J.; Tokarová, V.; Wichterlová, B. Incorporation of Al at ZSM-5 Hydrothermal Synthesis. Tuning of Al Pairs in the Framework. *Microporous Mesoporous Mater.* **2015**, *202*, 138−146.
(121) Vollmer, I.; Li, G.; Yarulina, I.; Kosinov, N.; Hensen, E. J. M.; Houben, K.; Mance, D.; Baldus, M.; Gascon, J.; Kapteijn, F. Relevance of the Mo-Precursor State in H-ZSM-5 for Methane Dehydroaromatization. *Catal. Sci. Technol.* **2018**, *8*, 916−922.
(122) Sazama, P.; Tabor, E.; Klein, P.; Wichterlova, B.; Sklenak, S.; Mokrzycki, L.; Pashkkova, V.; Ogura, M.; Dedecek, J. Al-Rich Beta Zeolites. Distribution of Al Atoms in the Framework and Related Protonic and Metal-Ion Species. *J. Catal.* **2016**, *333*, 102−114.
(123) Paolucci, C.; Parekh, A. A.; Khurana, I.; Di Iorio, J. R.; Li, H.; Albarracin Caballero, J. D.; Shih, A. J.; Anggara, T.; Delgass, W. N.; Miller, J. T.; Ribeiro, F. H.; Gounder, R.; Schneider, W. F. Catalysis in a Cage: Condition-Dependent Speciation and Dynamics of Exchanged Cu Cations in Ssz-13 Zeolites. *J. Am. Chem. Soc.* **2016**, *138*, 6028−6048.
(124) Tsai, T.; Liu, S.; Wang, I. Disproportionation and Transalkylation of Alkylbenzenes over Zeolite Catalysts. *Appl. Catal., A* **1999**, *181*, 355−398.
(125) Okamoto, M. Synthesis of Core-Shell Structured Porous Materials and Applications as Catalysts and Precursors for Hollow Porous Materials. *J. Jpn. Pet. Inst.* **2013**, *56*, 198−205.
(126) Ghorbanpour, A.; Gumidyala, A.; Grabow, L. C.; Crossley, S. P.; Rimer, J. D. Epitaxial Growth of ZSM-5@Silicalite-1: A Core-Shell Zeolite Designed with Passivated Surface Acidity. *ACS Nano* **2015**, *9*, 4006−4016.
(127) Bouizi, Y.; Rouleau, L.; Valtchev, V. P. Factors Controlling the Formation of Core-Shell Zeolite-Zeolite Composites. *Chem. Mater.* **2006**, *18*, 4959−4966.
(128) Du, T.; Qu, H.; Liu, Q.; Zhong, Q.; Ma, W. Synthesis, Activity and Hydrophobicity of Fe-ZSM-5 at Silicalite-1 for NH_3-SCR. *Chem. Eng. J.* **2015**, *262*, 1199−1207.
(129) Jin, Z.; Liu, S.; Qin, L.; Liu, Z.; Wang, Y.; Xie, Z.; Wang, X. Methane Dehydroaromatization by Mo-Supported MFI-Type Zeolite with Core-Shell Structure. *Appl. Catal., A* **2013**, *453*, 295−301.
(130) Groen, J. C.; Zhu, W.; Brouwer, S.; Huynink, S. J.; Kapteijn, F.; Moulijn, J. A.; Pérez-Ramírez, J. Direct Demonstration of Enhanced Diffusion in Mesoporous ZSM-5 Zeolite Obtained via Controlled Desilication. *J. Am. Chem. Soc.* **2007**, *129*, 355−360.
(131) Hartmann, M.; Machoke, G.; Schwieger, W. Catalytic Test Reactions for the Evaluation of Hierarchical Zeolites. *Chem. Soc. Rev.* **2016**, *45*, 3313−3330.
(132) Serrano, D. P.; Escola, J. M.; Pizarro, P. Synthesis Strategies in the Search for Hierarchical Zeolites. *Chem. Soc. Rev.* **2013**, *42*, 4004−4035.
(133) Valtchev, V.; Balanzat, E.; Mavrodinova, V.; Diaz, I.; El Fallah, J.; Goupil, J. M. High Energy Ion Irradiation-Induced Ordered Macropores in Zeolite Crystals. *J. Am. Chem. Soc.* **2011**, *133*, 18950−18956.
(134) Groen, J. C.; Moulijn, J. A.; Pérez-Ramírez, J. Desilication: On the Controlled Generation of Mesoporosity in MFI Zeolites. *J. Mater. Chem.* **2006**, *16*, 2121−2131.
(135) Peréz-Ramírez, J.; Verboekend, D.; Bonilla, A.; Abelló, S. Zeolite Catalysts with Tunable Hierarchy Factor by Pore-Growth Moderators. *Adv. Funct. Mater.* **2009**, *19*, 3972−3979.
(136) Verboekend, D.; Pérez-Ramírez, J. Design of Hierarchical Zeolite Catalysts by Desilication. *Catal. Sci. Technol.* **2011**, *1*, 879−890.
(137) Egeblad, K.; Christensen, C. H.; Kustova, M.; Christensen, C. H. Templating Mesoporous Zeolites. *Chem. Mater.* **2008**, *20*, 946−960.
(138) Sachse, A.; García-Martínez, J. Surfactant-Templating of Zeolites: From Design to Application. *Chem. Mater.* **2017**, *29*, 3827−3853.
(139) Choi, M.; Cho, H. S.; Srivastava, R.; Venkatesan, C.; Choi, D.-H.; Ryoo, R. Amphiphilic Organosilane-Directed Synthesis of Crystalline Zeolite with Tunable Mesoporosity. *Nat. Mater.* **2006**, *5*, 718−723.
(140) Choi, M.; Na, K.; Kim, J.; Sakamoto, Y.; Terasaki, O.; Ryoo, R. Stable Single-Unit-Cell Nanosheets of Zeolite MFI as Active and Long-Lived Catalysts. *Nature* **2009**, *461*, 828−828.
(141) Na, K.; Jo, C.; Kim, J.; Cho, K.; Jung, J.; Seo, Y.; Messinger, R. J.; Chmelka, B. F.; Ryoo, R. Directing Zeolite Structures into Hierarchically Nanoporous Architectures. *Science* **2011**, *333*, 328−332.
(142) Jiang, J.; Jorda, J. L.; Yu, J.; Baumes, L. A.; Mugnaioli, E.; Diaz-Cabanas, M. J.; Kolb, U.; Corma, A. Synthesis and Structure Determination of the Hierarchical Meso-Microporous Zeolite ITQ-43. *Science* **2011**, *333*, 1131−1134.
(143) Wu, L.; Degirmenci, V.; Magusin, P. C. M. M.; Szyja, B. M.; Hensen, E. J. M. Dual Template Synthesis of a Highly Mesoporous SSZ-13 Zeolite with Improved Stability in the Methanol-to-Olefins Reaction. *Chem. Commun.* **2012**, *48*, 9492−9494.
(144) Xu, L.; Ji, X.; Li, S.; Zhou, Z.; Du, X.; Sun, J.; Deng, F.; Che, S.; Wu, P. Self-Assembly of Cetyltrimethylammonium Bromide and Lamellar Zeolite Precursor for the Preparation of Hierarchical MWW Zeolite. *Chem. Mater.* **2016**, *28*, 4512−4521.
(145) Liu, B.; Tan, Y.; Ren, Y.; Li, C.; Xi, H.; Qian, Y. Fabrication of a Hierarchically Structured Beta Zeolite by a Dual-Porogenic Surfactant. *J. Mater. Chem.* **2012**, *22*, 18631−18638.
(146) Rani, P.; Srivastava, R.; Satpati, B. One-Step Dual Template Mediated Synthesis of Nanocrystalline Zeolites of Different Framework Structures. *Cryst. Growth Des.* **2016**, *16*, 3323−3333.
(147) Zhu, X.; Rohling, R.; Filonenko, G.; Mezari, B.; Hofmann, J. P.; Asahina, S.; Hensen, E. J. M. Synthesis of Hierarchical Zeolites Using an Inexpensive Mono-Quaternary Ammonium Surfactant as Mesoporogen. *Chem. Commun.* **2014**, *50*, 14658−14661.

DOI: 10.1021/acs.chemmater.8b01311
Chem. Mater. 2018, 30, 3177−3198

(148) Rani, P.; Satpati, B.; Srivastava, R. Natural Template Mediated Sustainable Synthesis of Nanocrystalline Zeolite with Significantly Improved Catalytic Activity. *ChemistrySelect* **2017**, *2*, 2870−2879.
(149) Meng, L.; Mezari, B.; Goesten, M. G.; Hensen, E. J. M. One-Step Synthesis of Hierarchical ZSM-5 Using Cetyltrimethylammonium as Mesoporogen and Structure-Directing Agent. *Chem. Mater.* **2017**, *29*, 4091−4096.
(150) Gallego, E. M.; Paris, C.; Díaz-Rey, M. R.; Martínez-Armero, M. E.; Martínez-Triguero, J.; Martínez, C.; Moliner, M.; Corma, A. Simple Organic Structure Directing Agents for Synthesizing Nanocrystalline Zeolites. *Chem. Sci.* **2017**, *8*, 8138−8149.
(151) Zhu, X.; Kosinov, N.; Hofmann, J. P.; Mezari, B.; Qian, Q.; Rohling, R.; Weckhuysen, B. M.; Ruiz-Martínez, J.; Hensen, E. J. M. Fluoride-Assisted Synthesis of Bimodal Microporous SSZ-13 Zeolite. *Chem. Commun.* **2016**, *52*, 3227−3230.
(152) Zhang, X.; Liu, D.; Xu, D.; Asahina, S.; Cychosz, K. A.; Agrawal, K. V.; Al Wahedi, Y.; Bhan, A.; Al Hashimi, S.; Terasaki, O.; Thommes, M.; Tsapatsis, M. Synthesis of Self-Pillared Zeolite Nanosheets by Repetitive Branching. *Science* **2012**, *336*, 1684−1687.
(153) Zhu, X.; Goesten, M. G.; Koekkoek, A.; Mezari, B.; Filonenko, G.; Friedrich, H.; Rohling, R.; Szyja, B. M.; Gascon, J.; Kapteijn, F.; Hensen, E. J. M.; Kosinov, N. Establishing Hierarchy: The Chain of Events Leading to the Formation of Silicalite-1 Nanosheets. *Chem. Sci.* **2016**, *7*, 6506−6513.
(154) Na, K.; Choi, M.; Ryoo, R. Recent Advances in the Synthesis of Hierarchically Nanoporous Zeolites. *Microporous Mesoporous Mater.* **2013**, *166*, 3−19.
(155) Schmidt, J. E.; Whiting, G. T.; Chowdhury, A. D.; Seoane, B.; Weckhuysen, B. M. Spectroscopy of Zeolites. In *Zeolites in Catalysis*; Royal Society of Chemistry: Cambridge, U.K., 2017; pp 240−276.
(156) Hoffman, A. S.; Fang, C. Y.; Gates, B. C. Homogeneity of Surface Sites in Supported Single-Site Metal Catalysts: Assessment with Band Widths of Metal Carbonyl Infrared Spectra. *J. Phys. Chem. Lett.* **2016**, *7*, 3854−3860.
(157) Serna, P.; Gates, B. C. Molecular Metal Catalysts on Supports: Organometallic Chemistry Meets Surface Science. *Acc. Chem. Res.* **2014**, *47*, 2612−2620.
(158) Chakrabarti, A.; Ford, M. E.; Gregory, D.; Hu, R.; Keturakis, C. J.; Lwin, S.; Tang, Y.; Yang, Z.; Zhu, M.; Bañares, M. A.; Wachs, I. E. A Decade+ of Operando Spectroscopy Studies. *Catal. Today* **2017**, *283*, 27−53.
(159) Weckhuysen, B. M. Determining the Active Site in a Catalytic Process: Operando Spectroscopy Is More than a Buzzword. *Phys. Chem. Chem. Phys.* **2003**, *5*, 4351−4360.
(160) Zhang, Y.; Fu, D.; Xu, X.; Sheng, Y.; Xu, J.; Han, Y. F. Application of Operando Spectroscopy on Catalytic Reactions. *Curr. Opin. Chem. Eng.* **2016**, *12*, 1−7.
(161) Miller, M. K.; Forbes, R. G. Atom Probe Tomography. *Mater. Charact.* **2009**, *60*, 461−469.
(162) Pidko, E. A.; Hensen, E. J. M. Computational Chemistry of Zeolite Catalysis. In *Zeolites and Zeolite-like Materials*; Elsevier B.V.: Amsterdam, 2016; pp 111−135.
(163) Nørskov, J. K.; Bligaard, T.; Rossmeisl, J.; Christensen, C. H. Towards the Computational Design of Solid Catalysts. *Nat. Chem.* **2009**, *1*, 37−46.
(164) Friedrich, H.; de Jongh, P. E.; Verkleij, A. J.; de Jong, K. P. Electron Tomography for Heterogeneous Catalysts and Related Nanostructured Materials Electron Tomography for Heterogeneous Catalysts and Related Nanostructured Materials. *Chem. Rev.* **2009**, *109*, 1613−1629.
(165) Labanowska, M. EPR Monitoring of Redox Processes in Transition Metal Oxide Catalysts. *ChemPhysChem* **2001**, *2*, 712−731.
(166) Brückner, A. Electron Paramagnetic Resonance: A Powerful Tool for Monitoring Working Catalysts. *Adv. Catal.* **2007**, *51*, 265−308.
(167) Millet, J.-M. M. Mössbauer Spectroscopy in Heterogeneous Catalysis. *Adv. Catal.* **2007**, *51*, 309−350.
(168) Blasco, T. Insights into Reaction Mechanisms in Heterogeneous Catalysis Revealed by in Situ NMR Spectroscopy. *Chem. Soc. Rev.* **2010**, *39*, 4685−4702.
(169) Copéret, C.; Liao, W. C.; Gordon, C. P.; Ong, T. C. Active Sites in Supported Single-Site Catalysts: An NMR Perspective. *J. Am. Chem. Soc.* **2017**, *139*, 10588−10596.
(170) Zheng, A.; Huang, S.-J.; Wang, Q.; Zhang, H.; Deng, F.; Liu, S.-B. Progress in Development and Application of Solid-State NMR for Solid Acid Catalysis. *Chin. J. Catal.* **2013**, *34*, 436−491.
(171) Cychosz, K. A.; Guillet-Nicolas, R.; García-Martínez, J.; Thommes, M. Recent Advances in the Textural Characterization of Hierarchically Structured Nanoporous Materials. *Chem. Soc. Rev.* **2017**, *46*, 389−414.
(172) Groen, J. C.; Peffer, L. A. A.; Pérez-Ramírez, J. Pore Size Determination in Modified Micro- and Mesoporous Materials. Pitfalls and Limitations in Gas Adsorption Data Analysis. *Microporous Mesoporous Mater.* **2003**, *60*, 1−17.
(173) Bhatia, S.; Beltramini, J.; Do, D. D. Temperature Programmed Analysis and Its Applications in Catalytic Systems. *Catal. Today* **1990**, *7*, 309−438.
(174) Jentoft, F. C. Ultraviolet−Visible−Near Infrared Spectroscopy in Catalysis: Theory, Experiment, Analysis, and Application Under Reaction Conditions. In *Advances in Catalysis*, 1st ed.; Elsevier Inc.: Amsterdam, 2009; Vol. *52*.
(175) Bordiga, S.; Lamberti, C.; Bonino, F.; Travert, A.; Thibault-Starzyk, F. Probing Zeolites by Vibrational Spectroscopies. *Chem. Soc. Rev.* **2015**, *44*, 7262−7341.
(176) Stavitski, E.; Weckhuysen, B. M. Infrared and Raman Imaging of Heterogeneous Catalysts. *Chem. Soc. Rev.* **2010**, *39*, 4615−4625.
(177) Bañares, M. A.; Mestl, G. Structural Characterization of Operating Catalysts by Raman Spectroscopy. In *Advances in Catalysis*; Elsevier Inc.: Amsterdam, 2009; Vol. *52*, pp 43−128.
(178) van Bokhoven, J. A.; Lamberti, C. Structure of Aluminum, Iron, and Other Heteroatoms in Zeolites by X-Ray Absorption Spectroscopy. *Coord. Chem. Rev.* **2014**, *277*−*278*, 275−290.
(179) De Groot, F. High-Resolution X-Ray Emission and X-Ray Absorption Spectroscopy. *Chem. Rev.* **2001**, *101*, 1779−1808.
(180) Bazin, D.; Guczi, L. Soft X-Ray Absorption Spectroscopy in Heterogeneous Catalysis. *Appl. Catal., A* **2001**, *213*, 147−162.
(181) Baraldi, A.; Comelli, G.; Lizzit, S.; Kiskinova, M.; Paolucci, G. Real-Time X-Ray Photoelectron Spectroscopy of Surface Reactions. *Surf. Sci. Rep.* **2003**, *49*, 169−224.
(182) Ingham, B. X-Ray Scattering Characterisation of Nanoparticles. *Crystallogr. Rev.* **2015**, *21*, 229−303.
(183) van Rijn, R.; Ackermann, M. D.; Balmes, O.; Dufrane, T.; Geluk, A.; Gonzalez, H.; Isern, H.; De Kuyper, E.; Petit, L.; Sole, V. A.; Wermeille, D.; Felici, R.; Frenken, J. W. M. Ultrahigh Vacuum/High-Pressure Flow Reactor for Surface X-Ray Diffraction and Grazing Incidence Small Angle X-Ray Scattering Studies close to Conditions for Industrial Catalysis. *Rev. Sci. Instrum.* **2010**, *81*, 014101.
(184) Villa, A.; Dimitratos, N.; Chan-Thaw, C. E.; Hammond, C.; Veith, G. M.; Wang, D.; Manzoli, M.; Prati, L.; Hutchings, G. J. Characterisation of Gold Catalysts. *Chem. Soc. Rev.* **2016**, *45*, 4953−4994.
(185) Pennycook, S. J.; Lupini, A. R.; Varela, M.; Borisevich, A.; Peng, Y.; Oxley, M. P.; Van Benthem, K.; Chisholm, M. F. Scanning Transmission Electron Microscopy for Nanostructure Characterization. In *Scanning Microscopy for Nanotechnology: Techniques and Applications*; Springer: New York, 2006; pp 152−191.
(186) Gao, W.; Hood, Z. D.; Chi, M. Interfaces in Heterogeneous Catalysts: Advancing Mechanistic Understanding through Atomic-Scale Measurements. *Acc. Chem. Res.* **2017**, *50*, 787−795.
(187) Yang, D.; Xu, P.; Browning, N. D.; Gates, B. C. Tracking Rh Atoms in Zeolite HY: First Steps of Metal Cluster Formation and Influence of Metal Nuclearity on Catalysis of Ethylene Hydrogenation and Ethylene Dimerization. *J. Phys. Chem. Lett.* **2016**, *7*, 2537−2543.
(188) Gates, B. C.; Flytzani-Stephanopoulos, M.; Dixon, D. A.; Katz, A. Atomically Dispersed Supported Metal Catalysts: Perspectives and

DOI: 10.1021/acs.chemmater.8b01311
Chem. Mater. 2018, 30, 3177−3198

Suggestions for Future Research. *Catal. Sci. Technol.* **2017**, *7*, 4259−4275.
(189) Huang, B.; Bates, M.; Zhuang, X. Super-Resolution Fluorescence Microscopy. *Annu. Rev. Biochem.* **2009**, *78*, 993−1016.
(190) De Cremer, G.; Sels, B. F.; De Vos, D. E.; Hofkens, J.; Roeffaers, M. B. J. Fluorescence Micro(spectro)scopy as a Tool to Study Catalytic Materials in Action. *Chem. Soc. Rev.* **2010**, *39*, 4703−4717.
(191) Janssen, K. P. F.; De Cremer, G.; Neely, R. K.; Kubarev, A. V.; van Loon, J.; Martens, J. A.; De Vos, D. E.; Roeffaers, M. B. J.; Hofkens, J. Single Molecule Methods for the Study of Catalysis: From Enzymes to Heterogeneous Catalysts. *Chem. Soc. Rev.* **2014**, *43*, 990−1006.
(192) Roeffaers, M. B. J.; De Cremer, G.; Libeert, J.; Ameloot, R.; Dedecker, P.; Bons, A. J.; Bückins, M.; Martens, J. A.; Sels, B. F.; De Vos, D. E.; Hofkens, J. Super-Resolution Reactivity Mapping of Nanostructured Catalyst Particles. *Angew. Chem., Int. Ed.* **2009**, *48*, 9285−9289.
(193) Ristanović, Z.; Kerssens, M. M.; Kubarev, A. V.; Hendriks, F. C.; Dedecker, P.; Hofkens, J.; Roeffaers, M. B. J.; Weckhuysen, B. M. High-Resolution Single-Molecule Fluorescence Imaging of Zeolite Aggregates within Real-Life Fluid Catalytic Cracking Particles. *Angew. Chem., Int. Ed.* **2015**, *54*, 1836−1840.
(194) Ristanović, Z.; Kubarev, A. V.; Hofkens, J.; Roeffaers, M. B. J.; Weckhuysen, B. M. Single Molecule Nanospectroscopy Visualizes Proton-Transfer Processes within a Zeolite Crystal. *J. Am. Chem. Soc.* **2016**, *138*, 13586−13596.
(195) Zhu, X.; Kosinov, N.; Kubarev, A. V.; Bolshakov, A.; Mezari, B.; Valastyan, I.; Hofmann, J. P.; Roeffaers, M. B. J.; Sarkadi-Pribóczki, E.; Hensen, E. J. M. Probing the Influence of SSZ-13 Zeolite Pore Hierarchy in Methanol-to-Olefins Catalysis by Using Nanometer Accuracy by Stochastic Chemical Reactions Fluorescence Microscopy and Positron Emission Profiling. *ChemCatChem* **2017**, *9*, 3470−3477.
(196) Kubarev, A. V.; Janssen, K. P. F.; Roeffaers, M. B. J. Noninvasive Nanoscopy Uncovers the Impact of the Hierarchical Porous Structure on the Catalytic Activity of Single Dealuminated Mordenite Crystals. *ChemCatChem* **2015**, *7*, 3646−3650.
(197) Cerezo, A.; Clifton, P. H.; Galtrey, M. J.; Humphreys, C. J.; Kelly, T. F.; Larson, D. J.; Lozano-Perez, S.; Marquis, E. A.; Oliver, R. A.; Sha, G.; Thompson, K.; Zandbergen, M.; Alvis, R. L. Atom Probe Tomography Today. *Mater. Today* **2007**, *10*, 36−42.
(198) Kelly, T. F.; Larson, D. J. Atom Probe Tomography 2012. *Annu. Rev. Mater. Res.* **2012**, *42*, 1−31.
(199) Gault, B.; Moody, M. P.; De Geuser, F.; La Fontaine, A.; Stephenson, L. T.; Haley, D.; Ringer, S. P. Spatial Resolution in Atom Probe Tomography. *Microsc. Microanal.* **2010**, *16*, 99−110.
(200) Miller, M. K.; Kelly, T. F.; Rajan, K.; Ringer, S. P. The Future of Atom Probe Tomography. *Mater. Today* **2012**, *15*, 158−165.
(201) Perea, D. E.; Arslan, I.; Liu, J.; Ristanović, Z.; Kovarik, L.; Arey, B. W.; Lercher, J. A.; Bare, S. R.; Weckhuysen, B. M. Determining the Location and Nearest Neighbours of Aluminium in Zeolites with Atom Probe Tomography. *Nat. Commun.* **2015**, *6*, 7589.
(202) Schmidt, J. E.; Poplawsky, J. D.; Mazumder, B.; Attila, Ã.; Fu, D.; de Winter, D. A. M.; Meirer, F.; Bare, S. R.; Weckhuysen, B. M. Coke Formation in a Zeolite Crystal During the Methanol-to-Hydrocarbons Reaction as Studied with Atom Probe Tomography. *Angew. Chem., Int. Ed.* **2016**, *55*, 11173−11177.
(203) Schmidt, J. E.; Oord, R.; Guo, W.; Poplawsky, J. D.; Weckhuysen, B. M. Nanoscale Tomography Reveals the Deactivation of Automotive Copper-exchanged Zeolite Catalysts. *Nat. Commun.* **2017**, *8*, 1666.
(204) Singh, J.; Lamberti, C.; van Bokhoven, J. A. Advanced X-Ray Absorption and Emission Spectroscopy: In Situ Catalytic Studies. *Chem. Soc. Rev.* **2010**, *39*, 4754−4766.
(205) Gibson, E. K.; Stere, C. E.; Curran-McAteer, B.; Jones, W.; Cibin, G.; Gianolio, D.; Goguet, A.; Wells, P. P.; Catlow, C. R. A.; Collier, P.; Hinde, P.; Hardacre, C. Probing the Role of a Non-Thermal Plasma (NTP) in the Hybrid NTP Catalytic Oxidation of Methane. *Angew. Chem., Int. Ed.* **2017**, *56*, 9351−9355.
(206) Newville, M. Fundamentals of XAFS. *Rev. Mineral. Geochem.* **2014**, *78*, 33−74.
(207) Ramaker, D. E.; Koningsberger, D. C. The Atomic AXAFS and $\Delta\mu$ XANES Techniques as Applied to Heterogeneous Catalysis and Electrocatalysis. *Phys. Chem. Chem. Phys.* **2010**, *12*, 5514−5534.
(208) Nelson, R. C.; Miller, J. T. An Introduction to X-Ray Absorption Spectroscopy and Its in Situ Application to Organometallic Compounds and Homogeneous Catalysts. *Catal. Sci. Technol.* **2012**, *2*, 461−470.
(209) Alp, E. E.; Mini, S. M.; Ramanathan, M. X-Ray Absorption Spectroscopy: EXAFS and XANES - A Versatile Tool to Study the Atomic and Electronic Structure of Materials. In *Synchchrotron X-ray Sources and New Opportunities in the Soil and Environmental Sciences*; Argonne National Laboratory, U.S. DOE, U.S. Government Printing Office: Washington, DC, 1990; pp 25−36.
(210) Chen, L. X.; Zhang, X.; Shelby, M. L. Recent Advances on Ultrafast X-Ray Spectroscopy in the Chemical Sciences. *Chem. Sci.* **2014**, *5*, 4136−4152.
(211) Bordiga, S.; Groppo, E.; Agostini, G.; van Bokhoven, J. A.; Lamberti, C. Reactivity of Surface Species in Heterogeneous Catalysts Probed by in Situ X-Ray Absorption Techniques. *Chem. Rev.* **2013**, *113*, 1736−1850.
(212) Glatzel, P.; Sikora, M.; Smolentsev, G.; Fernández-García, M. Hard X-Ray Photon-in Photon-out Spectroscopy. *Catal. Today* **2009**, *145*, 294−299.
(213) Glatzel, P.; Bergmann, U. High Resolution 1s Core Hole X-Ray Spectroscopy in 3d Transition Metal Complexes - Electronic and Structural Information. *Coord. Chem. Rev.* **2005**, *249*, 65−95.
(214) Martini, A.; Borfecchia, E.; Lomachenko, K. A.; Pankin, I.; Negri, C.; Berlier, G.; Beato, P.; Falsig, H.; Bordiga, S.; Lamberti, C. Composition-Driven Cu-Speciation and Reducibility in Cu-CHA Zeolite Catalysts: A Multivariate XAS/FTIR Approach to Complexity. *Chem. Sci.* **2017**, *8*, 6836−6851.
(215) Borfecchia, E.; Lomachenko, K. A.; Giordanino, F.; Falsig, H.; Beato, P.; Soldatov, A. V.; Bordiga, S.; Lamberti, C. Revisiting the Nature of Cu Sites in the Activated Cu-SSZ-13 Catalyst for SCR Reaction. *Chem. Sci.* **2015**, *6*, 548−563.
(216) Lomachenko, K. A.; Borfecchia, E.; Negri, C.; Berlier, G.; Lamberti, C.; Beato, P.; Falsig, H.; Bordiga, S. The Cu-CHA deNOx Catalyst in Action: Temperature-Dependent NH3-Assisted Selective Catalytic Reduction Monitored by Operando XAS and XES. *J. Am. Chem. Soc.* **2016**, *138*, 12025−12028.
(217) Ivanova, I. I.; Kolyagin, Y. G. Impact of in Situ MAS NMR Techniques to the Understanding of the Mechanisms of Zeolite Catalyzed Reactions. *Chem. Soc. Rev.* **2010**, *39*, 5018−5050.
(218) Rossini, A. J.; Zagdoun, A.; Lelli, M.; Lesage, A.; Copéret, C.; Emsley, L. Dynamic Nuclear Polarization Surface Enhanced NMR Spectroscopy. *Acc. Chem. Res.* **2013**, *46*, 1942−1951.
(219) Song, C.; Hu, K. N.; Joo, C. G.; Swager, T. M.; Griffin, R. G. TOTAPOL: A Biradical Polarizing Agent for Dynamic Nuclear Polarization Experiments in Aqueous Media. *J. Am. Chem. Soc.* **2006**, *128*, 11385−11390.
(220) Matsuki, Y.; Fujiwara, T. Advances in High-Field DNP Methods. In *Experimental Approaches of NMR Spectroscopy*; Springer: Singapore, 2017; pp 91−134.
(221) Ong, T. C.; Liao, W. C.; Mougel, V.; Gajan, D.; Lesage, A.; Emsley, L.; Copéret, C. Atomistic Description of Reaction Intermediates for Supported Metathesis Catalysts Enabled by DNP SENS. *Angew. Chem., Int. Ed.* **2016**, *55*, 4743−4747.
(222) Blanc, F. Acidity Strength of Solid Catalysts Probed by Hyperpolarized Natural Abundance ^{17}O NMR Spectroscopy. *Angew. Chem., Int. Ed.* **2017**, *56*, 11694−11696.
(223) Mance, D.; van der Zwan, J.; Velthoen, M. E. Z.; Meirer, F.; Weckhuysen, B. M.; Baldus, M.; Vogt, E. T. C. A DNP-Supported Solid-State NMR Study of Carbon Species in Fluid Catalytic Cracking Catalysts. *Chem. Commun.* **2017**, *53*, 3933−3936.
(224) Wolf, P.; Valla, M.; Rossini, A. J.; Comas-Vives, A.; Núñez-Zarur, F.; Malaman, B.; Lesage, A.; Emsley, L.; Copéret, C.; Hermans,

DOI: 10.1021/acs.chemmater.8b01311
Chem. Mater. 2018, 30, 3177−3198

I. NMR Signatures of the Active Sites in Sn-β Zeolite. *Angew. Chem., Int. Ed.* **2014**, *53*, 10179−10183.
(225) Harris, J. W.; Liao, W.-C.; Di Iorio, J. R.; Henry, A. M.; Ong, T.-C.; Comas-Vives, A.; Copéret, C.; Gounder, R. Molecular Structure and Confining Environment of Sn Sites in Single-Site Chabazite Zeolites. *Chem. Mater.* **2017**, *29*, 8824−8837.
(226) Gunther, W. R.; Michaelis, V. K.; Caporini, M. A.; Griffin, R. G.; Román-Leshkov, Y. Dynamic Nuclear Polarization NMR Enables the Analysis of Sn-Beta Zeolite Prepared with Natural Abundance ^{119}Sn Precursors. *J. Am. Chem. Soc.* **2014**, *136*, 6219−6222.
(227) Sandoval-Díaz, L. E.; González-Amaya, J. A.; Trujillo, C. A. General Aspects of Zeolite Acidity Characterization. *Microporous Mesoporous Mater.* **2015**, *215*, 229−243.
(228) Hadjiivanov, K. I. Identification of Neutral and Charged N_xO_y Surface Species by IR Spectroscopy. *Catal. Rev.: Sci. Eng.* **2000**, *42*, 71−144.
(229) Sushkevich, V. L.; Palagin, D.; Ranocchiari, M.; van Bokhoven, J. A. Selective Anaerobic Oxidation of Methane Enables Direct Synthesis of Methanol. *Science* **2017**, *356*, 523−527.
(230) Wachs, I. E.; Roberts, C. A. Monitoring Surface Metal Oxide Catalytic Active Sites with Raman Spectroscopy. *Chem. Soc. Rev.* **2010**, *39*, 5002−5017.
(231) Pidko, E. A.; van Santen, R. A. In *Zeolites and Catalysis*; Wiley-VCH Verlag GmbH & Co. KGaA: Weinheim, Germany, 2010; pp 301−334.
(232) van Speybroeck, V.; Hemelsoet, K.; Joos, L.; Waroquier, M.; Bell, R. G.; Catlow, C. R. A. Advances in Theory and Their Application within the Field of Zeolite Chemistry. *Chem. Soc. Rev.* **2015**, *44*, 7044−7111.
(233) Li, G.; Liu, C.; Rohling, R.; Hensen, E. J. M.; Pidko, E. A. In *Modelling and Simulation in the Science of Micro- and Meso-Porous Materials*; Van Speybroeck, V., van Santen, R. A., Eds.; Elsevier: Amsterdam, 2018; pp 229−263.
(234) Pidko, E. A.; Hensen, E. J. M.; van Santen, R. A. Self-Organization of Extraframework Cations in Zeolites. *Proc. R. Soc. London, Ser. A* **2012**, *468*, 2070−2086.
(235) Pidko, E. A.; Hensen, E. J. M.; Zhidomirov, G. M.; van Santen, R. A. Non-Localized Charge Compensation in Zeolites: A Periodic DFT Study of Cationic Gallium-Oxide Clusters in Mordenite. *J. Catal.* **2008**, *255*, 139−143.
(236) Pidko, E. A.; van Santen, R. A.; Hensen, E. J. M. Multinuclear Gallium-Oxide Cations in High-Silica Zeolites. *Phys. Chem. Chem. Phys.* **2009**, *11*, 2893−2902.
(237) Li, G.; Pidko, E. A.; van Santen, R. A.; Li, C.; Hensen, E. J. M. Stability of Extraframework Iron-Containing Complexes in ZSM-5 Zeolite. *J. Phys. Chem. C* **2013**, *117*, 413−426.
(238) Liu, C.; Li, G.; Hensen, E. J. M.; Pidko, E. A. Nature and Catalytic Role of Extraframework Aluminum in Faujasite Zeolite: A Theoretical Perspective. *ACS Catal.* **2015**, *5*, 7024−7033.
(239) Li, G.; Vassilev, P.; Sanchez-Sanchez, M.; Lercher, J. A.; Hensen, E. J. M.; Pidko, E. A. Stability and Reactivity of Copper Oxo-Clusters in ZSM-5 Zeolite for Selective Methane Oxidation to Methanol. *J. Catal.* **2016**, *338*, 305−312.
(240) Kosinov, N.; Coumans, F. J. A. G.; Li, G.; Uslamin, E.; Mezari, B.; Wijpkema, A. S. G.; Pidko, E. A.; Hensen, E. J. M. Stable Mo/HZSM-5 Methane Dehydroaromatization Catalysts Optimized for High-Temperature Calcination-Regeneration. *J. Catal.* **2017**, *346*, 125−133.
(241) Paolucci, C.; Khurana, I.; Parekh, A. A.; Li, S.; Shih, A. J.; Li, H.; Di Iorio, J. R.; Albarracin-Caballero, J. D.; Yezerets, A.; Miller, J. T.; Delgass, W. N.; Ribeiro, F. H.; Schneider, W. F.; Gounder, R. SI-Dynamic Multinuclear Sites Formed by Mobilized Copper Ions in NO_x Selective Catalytic Reduction. *Science* **2017**, *357*, 898−903.
(242) Luo, H. Y.; Lewis, J. D.; Román-Leshkov, Y. Lewis Acid Zeolites for Biomass Conversion: Perspectives and Challenges on Reactivity, Synthesis, and Stability. *Annu. Rev. Chem. Biomol. Eng.* **2016**, *7*, 663−692.
(243) Ratnasamy, P.; Srinivas, D.; Knözinger, H. Active Sites and Reactive Intermediates in Titanium Silicate Molecular Sieves. *Adv. Catal.* **2004**, *48*, 1−169.
(244) Vayssilov, G. N. Structural and Physicochemical Features of Titanium Silicalites. *Catal. Rev.: Sci. Eng.* **1997**, *39*, 209−251.
(245) Dong, J.; Zhu, H.; Xiang, Y.; Wang, Y.; An, P.; Gong, Y.; Liang, Y.; Qiu, L.; Zheng, A.; Peng, X.; Lin, M.; Xu, G.; Guo, Z.; Chen, D. Toward a Unified Identification of Ti Location in the MFI Framework of High-Ti-Loaded TS-1: Combined EXAFS, XANES, and DFT Study. *J. Phys. Chem. C* **2016**, *120*, 20114−20124.
(246) Deka, R. C.; Nasluzov, V. A.; Ivanova Shor, E. A.; Shor, A. M.; Vayssilov, G. N.; Rösch, N. Comparison of All Sites for Ti Substitution in Zeolite TS-1 by an Accurate Embedded-Cluster Method. *J. Phys. Chem. B* **2005**, *109*, 24304−24310.
(247) Shetty, S.; Kulkarni, B. S.; Kanhere, D. G.; Goursot, A.; Pal, S. A Comparative Study of Structural, Acidic and Hydrophilic Properties of Sn−BEA with Ti−BEA Using Periodic Density Functional Theory. *J. Phys. Chem. B* **2008**, *112*, 2573−2579.
(248) Yang, G.; Pidko, E. A.; Hensen, E. J. M. Structure, Stability, and Lewis Acidity of Mono and Double Ti, Zr, and Sn Framework Substitutions in BEA Zeolites: A Periodic Density Functional Theory Study. *J. Phys. Chem. C* **2013**, *117*, 3976−3986.
(249) Li, G.; Pidko, E. A.; Hensen, E. J. M. Synergy between Lewis Acid Sites and Hydroxyl Groups for the Isomerization of Glucose to Fructose over Sn-Containing Zeolites: A Theoretical Perspective. *Catal. Sci. Technol.* **2014**, *4*, 2241−2250.
(250) Thang, H. V.; Frolich, K.; Shamzhy, M.; Eliášová, P.; Rubeš, M.; Čejka, J.; Bulánek, R.; Nachtigall, P. The Effect of the Zeolite Pore Size on the Lewis Acid Strength of Extra-Framework Cations. *Phys. Chem. Chem. Phys.* **2016**, *18*, 18063−18073.
(251) Liu, C.; Tranca, I.; van Santen, R. A.; Hensen, E. J. M.; Pidko, E. A. Scaling Relations for Acidity and Reactivity of Zeolites. *J. Phys. Chem. C* **2017**, *121*, 23520−23530.
(252) Bai, P.; Jeon, M. Y.; Ren, L.; Knight, C.; Deem, M. W.; Tsapatsis, M.; Siepmann, J. I. Discovery of Optimal Zeolites for Challenging Separations and Chemical Transformations Using Predictive Materials Modeling. *Nat. Commun.* **2015**, *6*, 5912.
(253) Gallego, E. M.; Portilla, M. T.; Paris, C.; León-Escamilla, A.; Boronat, M.; Moliner, M.; Corma, A. "Ab Initio" Synthesis of Zeolites for Preestablished Catalytic Reactions. *Science* **2017**, *355*, 1051−1054.
(254) Rohling, Y. R.; Uslamin, E.; Zijlstra, B.; Tranca, I. C.; Filot, I. A. W.; Hensen, E. J. M.; Pidko, E. A. An Active Alkali-Exchanged Faujasite Catalyst for Para-Xylene Production via the One-Pot Diels-Alder Cycloaddition/dehydration Reaction of 2,5-Dimethylfuran with Ethylene. *ACS Catal.* **2018**, *8*, 760−769.
(255) Gates, B. C. From Catalyst Preparation toward Catalyst Synthesis. *J. Catal.* **2015**, *328*, 72−74.

DOI: 10.1021/acs.chemmater.8b01311
Chem. Mater. 2018, 30, 3177−3198